1967

The structure and infrared spectra of the tetrahalobis (acetonitrile) niobium (IV) complexes

Thomas Anthony Dougherty
Iowa State University

67-8906

DOUGHERTY, Thomas Anthony, 1937-

THE STRUCTURE AND INFRARED SPECTRA OF THE TETRAHALOBIS(ACETONITRILE)NIOBIUM(IV) COMPLEXES.

Iowa State University of Science and Technology, Ph.D., 1967
Chemistry, inorganic

University Microfilms, Inc., Ann Arbor, Michigan

THE STRUCTURE AND INFRARED SPECTRA OF THE TETRAHALOBIS(ACETONITRILE)NIOBIUM(IV) COMPLEXES

by

Thomas Anthony Dougherty

A Dissertation Submitted to the
Graduate Faculty in Partial Fulfillment of
The Requirements for the Degree of
DOCTOR OF PHILOSOPHY

Major Subject: Physical Chemistry

Approved:

Signature was redacted for privacy.

In Charge of Major Work

Signature was redacted for privacy.

Head of Major Department

Signature was redacted for privacy.

Dean of Graduate College

Iowa State University
Of Science and Technology
Ames, Iowa

1967

TABLE OF CONTENTS

PART I. THE $NbBr_4(CH_3CN)_2$ STRUCTURE

INTRODUCTION

A great deal of interest has centered on the chemistry of the heavy (4d and 5d) transition metals of groups V, VI, and VII. Most of the literature however, pertains to their maximum oxidation states. This is largely due to the high reactivity and consequent difficulty in the preparation and the purification of compounds containing the metals in lower oxidation states.

Recently, a number of the lower valent halide complexes have been prepared by carrying out the reactions under inert atmosphere in nonaqueous solvents selected to avoid solvolysis (1-10). These lower valent compounds are of particular interest due to their unusual spectral and magnetic properties.

The Crystal Field theory, though successful in explaining the spectra of many compounds with $3d^n$ configurations, breaks down in application to $4d^n$ and $5d^n$ cases. Since the 4d and 5d electrons are less tightly bound than the 3d electrons, the crystal field splitting is higher and charge transfer states become important (11). This probably facilitates electron delocalization <u>via</u> the formation of molecular orbitals (12).

Moreover, recent calculations on $VF_6^=$ and $TiF_6^=$ show that π-bonding is very significant and must be included in a discussion of the bonding (13,14). Such bonding is well known in

MO^{2+} and MO_2^{3+}, their remarkable stability can be attributed to the π-character of the metal-oxygen bond (15,16).

Also, spin-orbit coupling, usually of secondary importance in complexes of 3d elements, becomes far more important *viz.* the one electron spin-orbit coupling constant varies as $\lambda_{5d} \sim 2\lambda_{4d} \sim 5\lambda_{3d}$ (17).

Molecular Orbital theory thus gives the most satisfactory account of the bonding in compounds of the heavier transition elements since it includes both σ and π-bonding, as well as spin-orbit coupling.

Previous workers in this laboratory (10) have shown that the Nb(IV) halides form relatively stable adducts, $NbX_4(CH_3CN)_2$ (X = Cl, Br, I), with acetonitrile. Dipole moment, molecular weight, conductance, electronic spectra, and magnetic susceptibility measurements were all consistent with the cis-monomeric formulation of the adducts. It was also deduced that π-bonding of the type pπ - dπ may be important in these compounds.

Because of the interesting bonding in $NbX_4 \cdot 2CH_3CN$ and because a detailed structure determination on a compound of this type has not been reported, this work was undertaken.

REVIEW OF PREVIOUS WORK

Torp (10) has reviewed the literature on niobium(IV) halides and their complexes prior to 1963 so this will not be repeated. For the sake of completeness, a brief review of work germane to this thesis will be included.

Niobium(IV) Halides

A number of workers (1,18-20) have prepared and studied the tetra-chloride, bromide, and iodide of niobium. They are best prepared by synproportionation reactions of niobium and its pentahalide. These reactions are carried out in sealed evacuated vessels with the products separated by vapor transport. The tetrahalides are diamagnetic, and are unstable toward hydrolysis and oxidation in the atmosphere. NbI_4 moreover appears to exist in three polymeric forms (21). This phenomenon has not been observed for the bromide or chloride.

A single crystal x-ray crystal structure determination (22) of the α-NbI_4 (low temperature form) showed it to be orthorhombic with lattice parameters $a = 7.67 \pm 0.02\text{Å}$, $b = 13.28 \pm 0.02\text{Å}$ and $c = 12.93 \pm 0.02\text{Å}$. The structure consists of infinite chains of NbI_6 octahedra sharing opposite sides. The niobium atoms are displaced from the octahedra centers, 3.83Å apart, such that the Nb-Nb distance is 3.2Å. This

displacement of the niobium atoms indicates metal-metal interaction and would explain the observed diamagnetism resulting from pairing of the electrons on adjacent metal atoms. McCarley and Torp (1) indicate that the chloride and bromide have similar structures.

Hexahalo Niobium(IV) Complexes

Although the existence of the $NbCl_6^=$ had been shown by many workers (23-25), Torp (10) first prepared and characterized pure compounds of the type A_2NbX_6 (A = K, Rb, Cs; X = Cl, Br, I). These were prepared in sealed evacuated vessels by reaction of the tetrahalide with the molten alkali metal halide.

A detailed structural investigation of K_2NbCl_6 showed these compounds have the antifluorite (K_2PtCl_6) structure with octahedral $MX_6^=$ ions at the corners and face centered positions of the unit cell and A^+ ions in the tetrahedral holes. Their lattice stability was shown to be a function of the cation/anion radius ratio.

The electronic absorption spectra of the A_2MX_6 complexes consists of two low intensity peaks at long wavelengths assigned to the d-d transition $t_{2g}^* \rightarrow e_g^*$, (split by Jahn-Teller distortion) and high intensity peaks assigned to halide $\rightarrow e_g^*$

and halide → t_{2g}^* charge transfer transitions.

Magnetic susceptibility studies yielded paramagnetic moments below the spin only value, with spin-orbit coupling constants ranging from 300-650 cm^{-1}. These data indicate appreciable $p\pi$ - $d\pi$ halide to metal bonding decreasing in the order Cl > Br > I.

Niobium(IV) Mixed Complexes

A number of complexes of the type $(BH)_2Nb(OR)Cl_5$ (OR = alkoxide; B = amine such as CH_3NH_2, pyridine or quinoline) have been investigated by Wentworth and Brubaker (6). These compounds were prepared by electrolytic reduction of $NbCl_5$ in HCl-saturated alcohols followed by the addition of alcoholic solutions of BH^+ ions. The experiments were carried out under nitrogen atmosphere. Magnetic susceptibilities of the complexes were measured as a function of temperature and found to obey the Curie-Weiss Law. The calculated moments correspond to the spin only value for the d^1 ion. The reflectance spectrum of $(CH_3NH_3)_2Nb(OEt)Cl_5$, measured in mineral oil, showed a single peak at 510 mμ. Brubaker *et al.* (26) measured the electron spin resonance spectrum of $Nb(OCH_3)Cl_5^=$ both in methanol solution (300°K) and in a frozen methanol glass (77°K). These workers report $\langle g \rangle = 1.861 \pm 0.002$ and $\langle a \rangle =$

178 ± 3 gauss. By comparison with results on the similar vanadyl ion (15), they estimate extensive π-bond interaction between the niobium atom and the four planar chlorine atoms.

Wentworth and Brubaker (7) also prepared the diamagnetic complexes $[Nb(OEt)_4]_n$ and $[NbCl(OEt)_3py]_2$ in ethyl alcohol. The diamagnetism of these compounds is explained in terms of direct metal-metal bonding between adjacent niobium ions.

McCarley et al. (1,2) prepared $NbX_4 \cdot 2$ pyridine (X = Cl, Br, I) by extraction of NbX_4 with pyridine at room temperature in vacuo. These compounds, formulated as monomers, are paramagnetic following a simple Curie relationship over the range -196 to 25°C. Their visible spectra in pyridine solutions consisted of at least two peaks of relatively high intensity ($\varepsilon \geq 500$) assigned to charge transfer transitions from the filled π-orbitals of pyridine to a non-bonding orbital on niobium.

Allbutt et al. (27) prepared complexes of the type $NbX_4 \cdot 2L$ (X = Cl, Br; L = pyridine, γ-picoline) by direct reaction of the amines with the corresponding pentahalides. They also prepared $NbCl_4 \cdot B$ (B = 1:10 phenanthroline,bipyridyl) by direct reaction with $NbCl_5$. These products closely resemble the pyridine adducts.

Torp (10) prepared $NbX_4 \cdot 2CH_3CN$ (X = Cl, Br, I) by extraction of the tetrahalides with acetonitrile *in vacuo* at room temperature. A solid of composition $NbCl_4 \cdot 3CH_3CN$ was found to be stable at room temperature. No such compound was found for the bromide or iodide analogs. Absorption spectra consisted of two low intensity peaks which were assigned as transitions between the components of the t_{2g}^* and e_g^* levels split in the low symmetry field. The high intensity peaks ($\epsilon > 1000$) at higher energies were assigned to ligand → metal charge transfer transitions. It was inferred from these spectra that there is little niobium-nitrogen π-bonding.

Clark *et al.* (28) prepared the eight coordinate niobium (IV) complexes $NbX_4 \cdot 2$Diarsine (X = Cl, Br, I; Diarsine = $C_6H_4[As(CH_3)_2]_2$) by reaction of the tetrahalide with Diarsine in sealed tubes at elevated temperatures. Electron spin resonance studies of the chloride complex gave an average g value of 1.951, and hence the near spin-only moment of 1.67 B.M. No studies of the temperature dependence of the magnetic susceptibility were possible, due to the presence of ferromagnetic decomposition products.

STRUCTURE ANALYSIS

Ease of accessibility to large fast computers is responsible for the great proliferation of crystallographic data in recent years. Today structures are being solved routinely which would not have been attempted even ten years ago. The $NbBr_4(CH_3CN)_2$ structure is of this type.

During the period of this investigation, the Ames Laboratory phased out the IBM 7074-1401 computer and began using the IBM 360-50. Many programs were written and used with each facility. Below are listed the major programs of this investigation, the computer on which they were used, and their principal authors.

IBM 7074-1401

SCO-6	Single Crystal Orienter Program. D. E. Williams (29)
Nightmare	Data Workup Program. T. A. Dougherty
Patt. Sharp.	Patterson Sharpening Program. B. Granoff (30)
Patterson 1	Generates three-dimensional Patterson Map. T. E. Johnston (31)
Veccheck	Generates Symmetry Map. D. Erbeck (32)
Abcorr.	Calculates absorption correction for polyhedral crystals. Busing and Levy (33)

IBM 360-50

ORLS	Structure factors and least squares calculations. Busing and Levy (34)

Fourier	Calculates Fourier and Fourier Difference Maps. D. E. Williams and T. A. Dougherty
ORFFE	Function and Error. Busing and Levy (35)
ORTEP	Plot Program for Crystal Structures. C. K. Johnson (36)

In addition to the above, numerous small programs were written and used by the author. The author greatly appreciates use of the above programs and of the Ames Laboratory computing facility.

In the least squares refinement technique, one seeks to minimize the function

$$\frac{\sum \omega_{hk\ell} \left| |F_o(hk\ell)| - |F_c(hk\ell)| \right|^2}{\sum \omega_{hk\ell} \; F_o(hk\ell)^2}$$

where $\omega_{hk\ell}$ is the weighting factor, $F_o(hk\ell)$ is the observed structure factor and $F_c(hk\ell)$ is the calculated structure factor of the $\{hk\ell\}$ reflection.

The choice of the weighting scheme determines the rate and extent of convergence, indeed whether the process converges at all. Thus it is of extreme importance that an intelligent choice of the weighting scheme be made. The weighting scheme chosen here is

$$\omega_{hk\ell} = 1/\sigma^2_{F(hk\ell)}$$

where $\sigma_{F(hk\ell)}$ is the standard deviation of the structure factor. The appropriateness of this choice will be discussed in a later section.

Structure Analysis Methods

In general, a crystal structure is solved by application of the "Heavy Atom" method, "Direct" methods, or "Image-Seeking" methods.

The "Heavy Atom" method is based on the premise that the majority of the signs of the structure factors will be correctly determined upon location of a few "heavy atoms" within the unit cell. Calculation of an electron density map using these signs will then aid one in the location of additional atoms of the structure. The heavy atom index is defined as $Z_H^2/\Sigma_L Z_L^2$ where Z_H and Z_L are the atomic numbers of the heavy and light atoms of the structure, respectively. This index should be in excess of 1/3 for reasonable application of this treatment (37). There is no atom in $NbBr_4(CH_3CN)_2$ that is truly heavy with respect to the rest of the molecule. Moreover this compound crystallizes in a non-centrosymmetric space group and such structures are particularly dependent upon the heaviness index since the phase factor as well as the sign must be

determined for each structure factor.

Direct methods are presently confined to centrosymmetric structures or projections so they too are inapplicable (38). It was therefore decided to solve this structure by the use of Image-Seeking methods. These methods involve reduction of the Patterson map to a single image of the structure in electron density space.

Wrinch (39) in 1939 was the first to suggest a method for the systematic analysis of vector distributions. The idea was rediscovered in 1950 by a number of investigators (40,41) but only became popular with the advent of high speed computers (42,43). The method of vector superpositions, augmented by the generation of a symmetry map, was selected for solution of this structure. A brief review of the Patterson synthesis, and of these methods, follows.

Patterson synthesis

The electron density function is defined as

$$\rho(x,y,z) = 1/V \sum_{h} \sum_{k} \sum_{\ell} F(hk\ell) \exp\left\{-2\pi i(hx+ky+\ell z)\right\}$$

where $F(hk\ell)$ is the structure factor of the reflection $\{hk\ell\}$ and V is the volume of the unit cell. The magnitudes of the F's are experimentally accessible through intensity measurements, but their signs are not. Since for twenty structure

factors there are well over one million possible sign combinations, the correct assignment of these signs is the problem of crystallography.

In 1934, Patterson (44) proposed the use of the self-convolution of the electron density function, e.g.

$$P(u,v,w) = \int_0^\infty \int_0^\infty \int_0^\infty \rho(xyz)\ \rho(x+u,y+v,z+w)\,V dx dy dz\ .$$

This may then be represented

$$P(u,v,w) = \frac{1}{V} \sum_h \sum_k \sum_\ell F(hk\ell)^2 \exp\left\{-2\pi i(hu+kv+\ell w)\right\}.$$

Thus it is similar to the electron density function except that only the structure factor magnitudes are needed for its evaluation.

The physical meaning of this quantity may be easily grasped from the defining equation. It is apparent that when $\underline{u}$ corresponds to an interatomic vector, $P(\underline{u})$ will be large, otherwise it will be small. One can also see that the magnitude of $P(\underline{u})$ is directly proportional to the product of the atomic numbers of the atoms related by the vector $\underline{u}$. The Patterson map is therefore a vector map of the unit cell with all vectors shifted to a common origin. As a consequence of this, all translational symmetry is lost. In an acentric structure of n atoms, the Patterson map contains n(n-1) non-

origin peaks. With symmetry elements present however, many of these peaks fall upon one another.

The $NbBr_4(CH_3CN)_2$ structure contains 1892 non-hydrogen peaks, i.e. approximately two per cubic Å of electron density space. The problem is to separate a single image of the unit cell from the forty-three others present.

Patterson superpositions

The Patterson superposition technique (45) affords a method of reducing a Patterson map to a single image of the structure in electron density space, i.e. of reducing a vector set to the corresponding fundamental set.

Consider an array of n atoms with vectors $\underline{A}_1, \underline{A}_2, \ldots \underline{A}_n$ drawn from an arbitrary origin to each atom. Then the Patterson is given by the set of vectors $[\underline{A}_j - \underline{A}_i]$, i = 1,n; j = 1,n. Now if a member of this set $[\underline{A}_\ell - \underline{A}_k]$ is added to the above set, a new Patterson with its origin shifted by this vector is produced. Then by comparing the two maps we find in common the sets

$$1) \quad [\underline{A}_j - \underline{A}_k] \qquad j = 1,n$$

$$2) \quad [\underline{A}_\ell - \underline{A}_i] \qquad i = 1,n$$

providing $[\underline{A}_\ell - \underline{A}_k]$ is a unique vector. Now 1) is merely the structure with the origin at A_k and 2) is the structure

inverse with the origin at A_ℓ. Following the same procedure with the new vector $[\underline{A}_m - \underline{A}_k]$ we again get two images, only one of which is common to all three maps. Utilizing this technique, one must eventually obtain a single image of the structure.

This technique is done in practice by the utilization of the minimum function of Buerger (46),

$$M_n(\underline{u}) = M_{in}[P(\underline{u}),\ P(\underline{u} - \underline{s}_1),\ P(\underline{u} - \underline{s}_r),\ ..,\ P(\underline{u} - \underline{s}_n)]r = 1,n$$

where $M_n(\underline{u})$ is the nth order minimum function, $P(\underline{u})$ is a three dimensional Patterson, and the $P(\underline{u} - \underline{s}_r)$ are Patterson maps shifted by the vector $\underline{s}_r$.

Figure 1(a) is a point structure in the plane Pg. Figure 1(b) is its corresponding Patterson map. The origin is marked with a square and all non-unique vectors are circles. Figure 2(a) represents the map obtained after a single superposition using the vector $[\underline{r}_8 - \underline{r}_3]$. The structure is delineated by solid lines, its inverse in dotted lines, and the center of symmetry by a plus sign. The remaining points are coincidences. The result of two superpositions is shown in Figure 2(b).

The coincidence points of Figure 2(a) result from the vectors $[\underline{r}_4 - \underline{r}_2]$, $[\underline{r}_4 - \underline{r}_1]$, $[\underline{r}_2 - \underline{r}_1]$ and their inverse

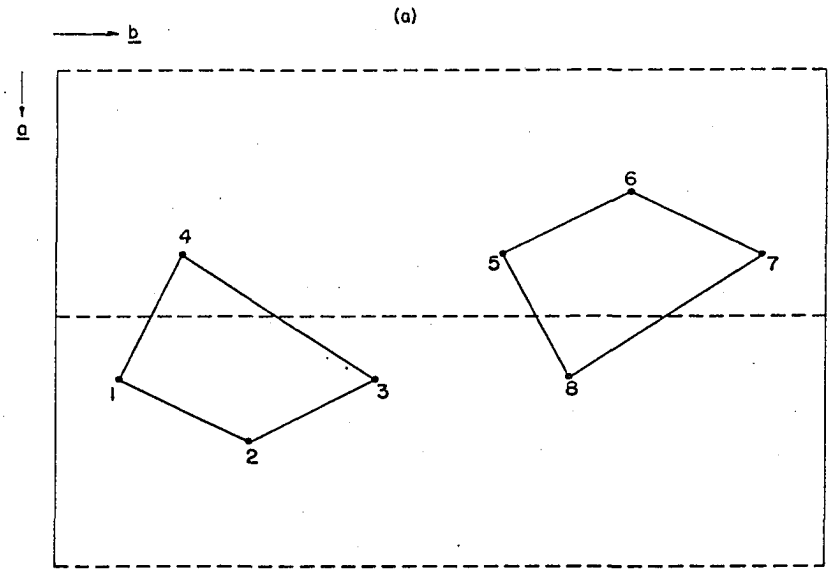

Figure 1a. Point structure in Pg space group

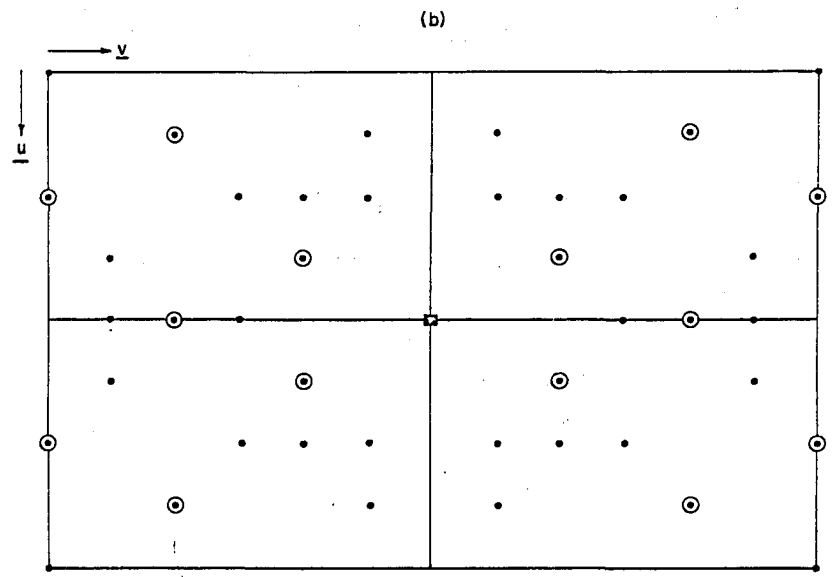

Figure 1b. Patterson map of point structure

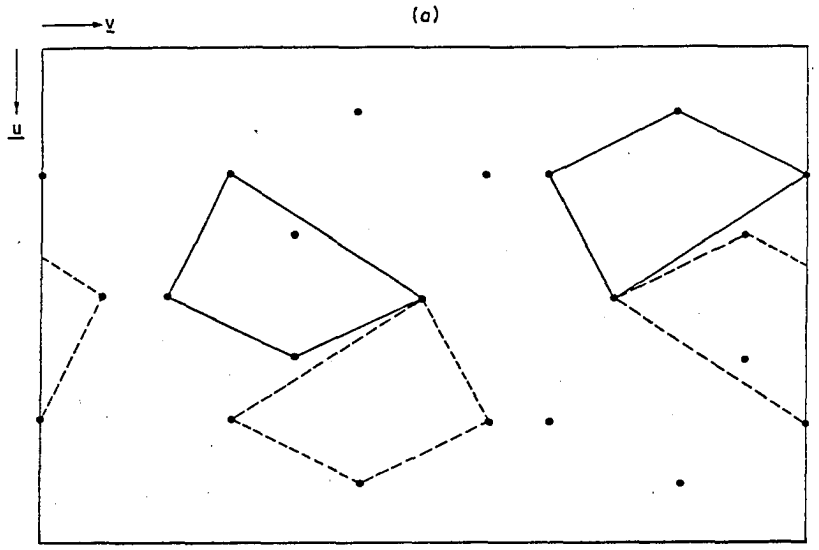

Figure 2a. Figure 1a following a superposition using the displacement [$\underline{r}_8 - \underline{r}_3$]

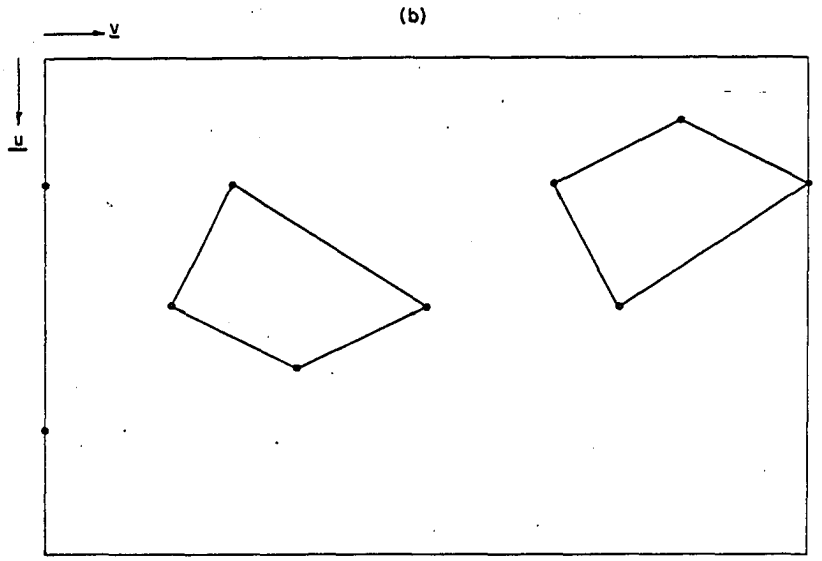

Figure 2b. Figure 1a following a superposition using the displacement [$\underline{r}_5 - \underline{r}_3$]

vectors. These points are termed "accidental" in that they are generated indirectly from the interpositional vectors of the structure. That they should remain is easily explained.

The function $M_1(\underline{u})$ retains peaks of the set $[\underline{r}_s - \underline{r}_t]$ such that

$$[\underline{r}_s - \underline{r}_t] = [\underline{r}_i - \underline{r}_j] + [\underline{r}_8 - \underline{r}_3] \in [\underline{r}_i - \underline{r}_j] \quad i = 1,8; \; j = 1,8.$$

However,

$$[\underline{r}_4 - \underline{r}_3] + [\underline{r}_8 - \underline{r}_3] = [\underline{r}_4 - \underline{r}_1] \in [\underline{r}_i - \underline{r}_j] ,$$

$$[\underline{r}_5 - \underline{r}_2] + [\underline{r}_8 - \underline{r}_3] = [\underline{r}_4 - \underline{r}_2] \in [\underline{r}_i - \underline{r}_j] ,$$

$$[\underline{r}_8 - \underline{r}_2] + [\underline{r}_8 - \underline{r}_3] = [\underline{r}_1 - \underline{r}_2] \in [\underline{r}_i - \underline{r}_j] ,$$

and similarly for the inverse vectors.

Thus, these peaks remain after a single superposition. These points are eliminated upon superpositions using the shift vector $[\underline{r}_5 - \underline{r}_3]$ in conjunction with the vector $[\underline{r}_8 - \underline{r}_3]$.

The symmetry map

A practical method of immediately simplifying the Patterson map was suggested by Mighell and Jacobson (48). Any accurate image of the structure must have the symmetry of the space group. This restriction may be applied to the Patterson using the interequivalent point vectors. Then, using the minimum function,

$$SM(\underline{u}) = M_{in} \; P(\underline{u} - \underline{a}_1), \ldots, P(\underline{u} - \underline{a}_s), \ldots, P(\underline{u} - \underline{a}_{n-1}) \quad \begin{matrix} s = 1, \\ n - 1 \end{matrix}$$

where n is the number of equivalent points of the space group. For the Pg group we have

$$SM(\underline{u}) = P(\underline{u} - \underline{a}),\ \underline{a} = (2x, \tfrac{1}{2}).$$

Figure 3(a) is the symmetry map for this space group and the Patterson of Figure 1.

Figure 3(b) is the result of a single Patterson superposition on this map. The original Patterson is reduced from 42 to 31 points. The simplification introduced by this technique is dependent upon the number of equivalent points of the space group used. The result of a single superposition of the Patterson upon the symmetry map using the $Pna2_1$ space group contained only 56 peaks of "strength" 150 or larger, a simplification of 95%.

Image-seeking functions do not work as well in practice as in theory. In reality, one is dealing with scatterers of finite size giving rise to continuous peaks in Patterson space. These peaks have volumes eight times those in electron density space. The overlap of these peaks coupled with their size guarantees the absence of nicely resolved peaks in the resultant electron density map. Modification functions are often used to sharpen the Patterson Map. A program written by B. Granoff was used in this investigation. Computer programs written by D. Erbeck

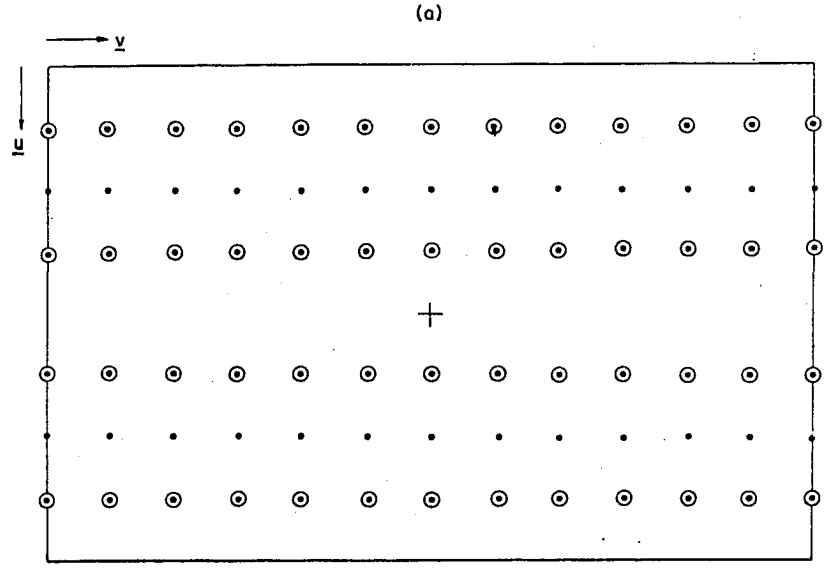

Figure 3a. Symmetry map of point structure

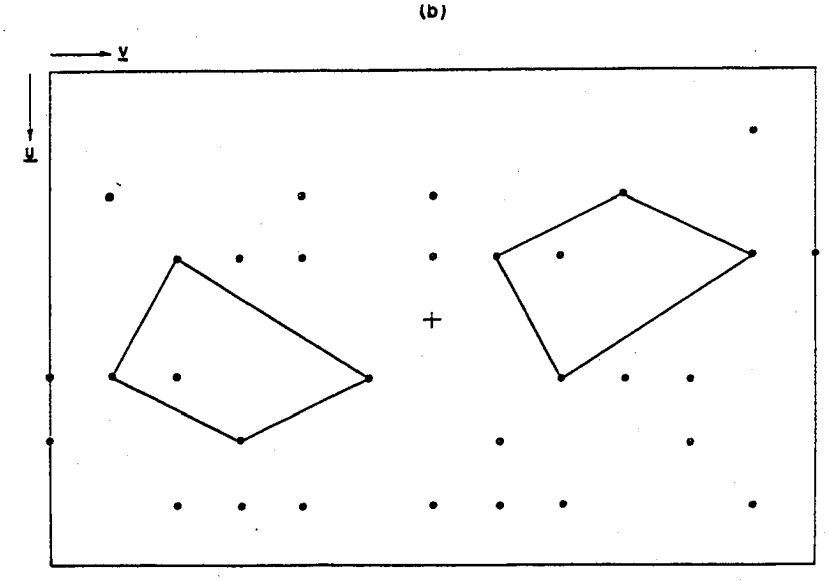

Figure 3b. Symmetry map following one superposition with the Patterson map at the origin

and T. Johnston were used in generation of the Patterson map, symmetry map, and the subsequent superpositions.

Space Group and Lattice Parameters

Zero, first, second and third layer Weissenberg pictures were taken and indexed. The Laue symmetry was later confirmed to be Pmmm. The systematic presences observed were:

$$\{ok\ell\} \qquad k + \ell = 2n$$

$$\{ho\ell\} \qquad h = 2n.$$

On the basis of these restrictions, the space group is either $Pna2_1$ or Pnam (47). No unique selection was possible at this time. The equivalent positions of these space groups are given in Tables 1 and 2.

Table 1. Equivalent positions of $Pna2_1$

No. of positions	Point symmetry	Equivalent positions
4	1	x,y,z; $\bar{x}$,$\bar{y}$,1/2+z 1/2-x,1/2+y,1/2+z; 1/2+x,1/2-y,z

Table 2. Equivalent positions of Pnam

No. of positions	Point symmetry	Equivalent positions	
4	m	$x,y,1/4$; $\bar{x},\bar{y},3/4$	
		$1/2-x,1/2-y,1/4$;	$1/2-x,1/2+y,3/4$
8	1	x,y,z	$\bar{x},\bar{y},\bar{z}$
		$x,y,1/2-z$	$\bar{x},\bar{y},1/2+z$
		$1/2+x,1/2-y,z$	$1/2-x,1/2+y,\bar{z}$
		$1/2+x,1/2-y,1/2-z$	$1/2-x,1/2+y,$ $1/2+z$

Precise lattice constants were measured directly from zero level precession pictures. The 6.00 cm crystal to film distance was confirmed by taking pictures of a standard NaCl crystal. The observed lattice parameters and their standard deviations are

$$a = 13.92 \pm 0.01\text{Å}$$

$$b = 6.58 \pm 0.01\text{Å}$$

$$c = 13.63 \pm 0.01\text{Å}.$$

Density was measured pycnometrically using chloroform for volume determinations. The observed value of 2.2 compared favorably with the value of 2.34 calculated for four formula weights per unit cell.

Preparation and Crystal Growth

The extreme reactivity of this compound coupled with a propensity to twinning caused great difficulties in single crystal preparation. Sealed and evacuated vessels or inert atmospheres were used in all preparations. All materials used in the preparations were rigorously dried and stored in evacuated containers. Storage and handling of materials were done in a dry-box under argon atmosphere. This dry-box was maintained at dew-point of ca. -70°C by a semi-constant flow of argon (dried over Linde 4A Molecular Sieves) through the box. In addition, argon within the box was constantly recycled over these drying agents to remove any remaining moisture.

Powdered $NbBr_4(CH_3CN)_2$ was kindly supplied by B. Torp of the Ames Laboratory. Single crystals were produced in the apparatus of Fig. 4. Solid $NbBr_4(CH_3CN)_2$ (ca. 0.5 g.) was placed on the frit and the apparatus evacuated. Five to ten mls. of CH_3CN were added by distillation, the apparatus inverted and placed in a constant temperature bath at 50°C for about 12 hours. The saturated solution was decanted through the frit and the apparatus placed in a gallon vessel of water heated to 50°C. This cooled slowly to room temperature over four to five hours. The solution was again decanted through

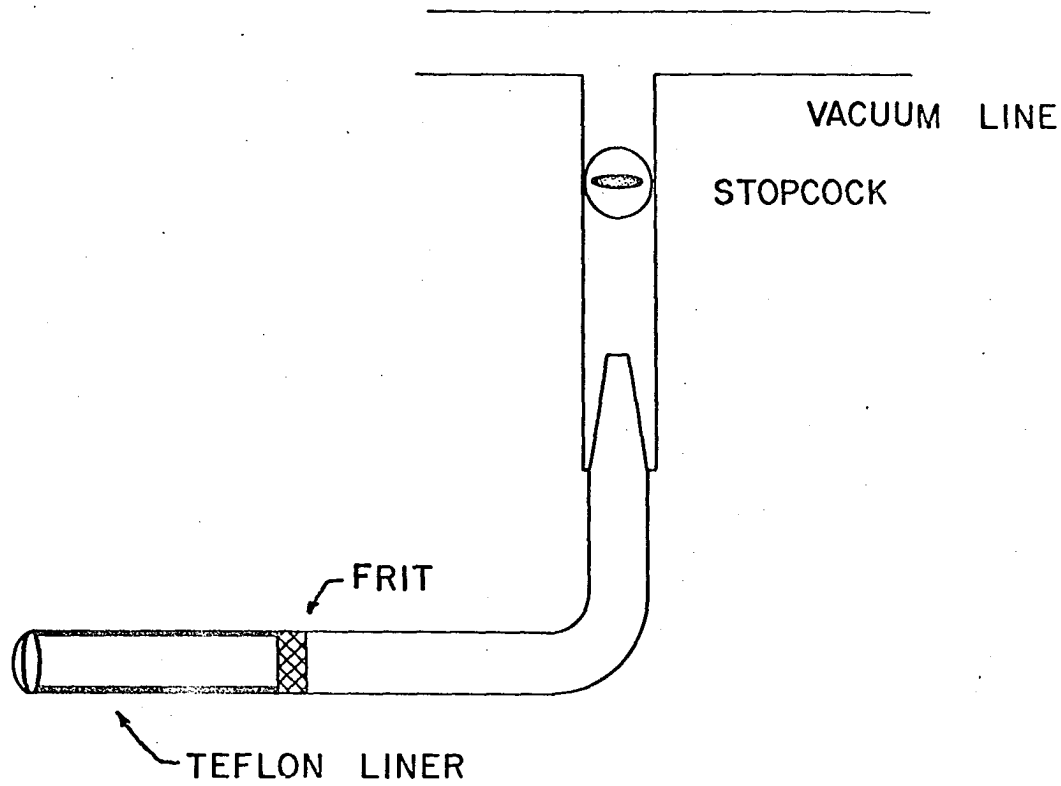

Figure 4. Apparatus for single-crystal growth

the frit and excess acetonitrile distilled off. The apparatus was then taken into the dry box, broken and any crystals removed. The Teflon coating was found essential to preserve the crystals as they shattered when removed from glass. Single crystals suitable for x-ray work were selected in a dry-box using a microscope, and were then sealed in capillaries.

Data Collection and Correction

Complete three-dimensional x-ray diffraction intensity data (up to $\sin \theta/\lambda = 0.5$) were taken from an irregular crystal of approximately 0.1 mm maximum dimensions. Molybdenum radiation with a zirconium filter was used (49). A General Electric XRD-5 x-ray unit equipped with a single crystal orienter and scintillation counter was used with the 2θ scan technique (50). A 200 second scan covering 3.33° in 2θ was used for each reflection followed by a repeat scan for background with an omega offset of 1.5°.

Three strong reflections (600), (020) and (002) were selected as standards and their intensities measured regularly throughout the period of data collection. These intensities were put on a common scale by dividing each intensity by the average intensity over the entire curve. These values were then averaged to obtain the curve of Figure 5. All measured

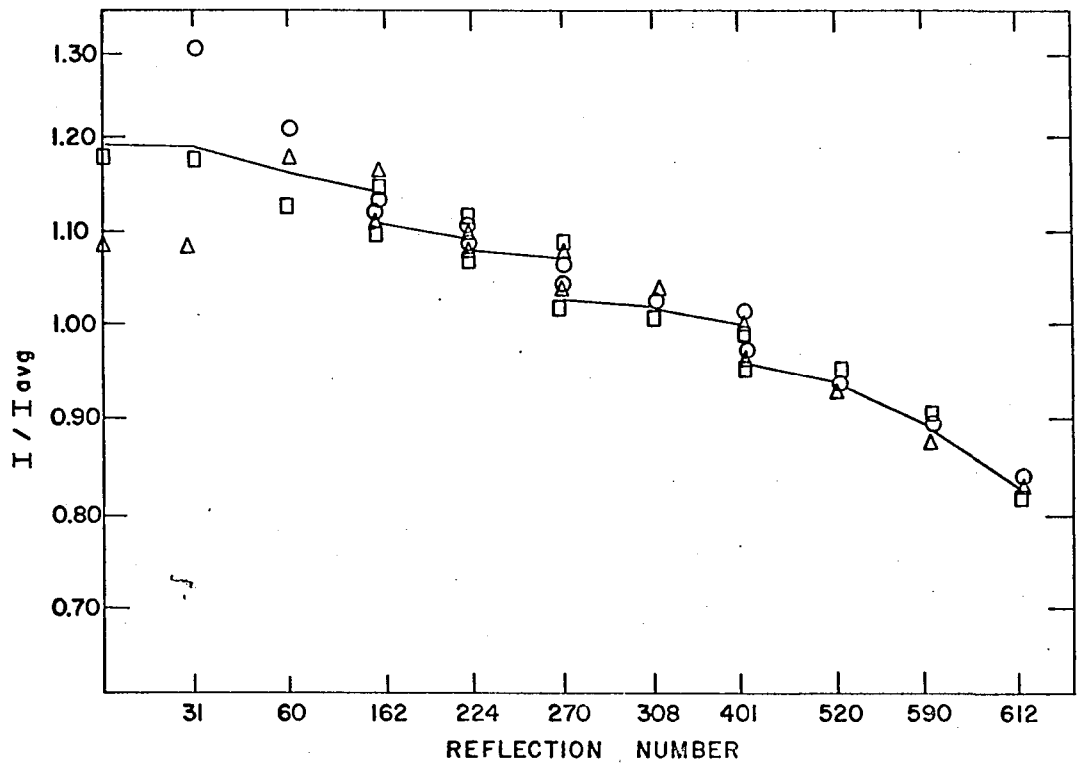

Figure 5. Decomposition curve

intensities were divided by the ordinate of this curve, placing them on a common scale. This variation is probably due to any or all of the following effects: decomposition of the crystal due to irradiation, a leak in the capillary, variation in the power supply, or variations in the response of the scintillation counter. A total of 612 intensities was measured.

Due to the high linear absorption coefficient of this compound (144 cm^{-1}) (51), an absorption correction was applied. The transmission coefficient is defined,

$$A = \frac{1}{V} \int_{V} \exp\left[-\mu(r_{\alpha} + r_{\beta})\right] dV,$$

where V is the volume of the crystal and r_{α} and r_{β} are the path lengths of the incident and diffracted beams. This integral cannot be integrated in closed form. The abcorr. program was used to evaluate the integral numerically using the Gaussian method. This program calculates transmission coefficients for polyhedra of arbitrary shape, given the linear absorption coefficient and the equations of the planes defining the crystal.

The crystal dimensions and orientation were measured using a microscope equipped with a filar eyepiece. Figures 6(a) and (b) show two views of the crystal with the angle settings of the orienter and the equations of the defining planes given

Boundary Plane Equations in cm.

I.			-1.000 z	+0.0308 = 0	VII.	0.2860 x -0.839 Y	+0.556 z -0.0217 = 0
II.	1.000 x			+0.0111 = 0	VIII.	1.000 x	-0.0111 = 0
III.	0.3486 x		+0.9373 z	+0.0264 = 0	IX.	0.991 x	-0.1345z -0.0113 = 0
IV.	0.3140 x	-0.950 Y		+0.0093 = 0	X.		-1.000 Y +0.0121 = 0
V.	0.3140 x	+0.950 Y		+0.0093 = 0	XI.		1.000 Y +0.0121 = 0
VI.	0.2860 x	+0.839 Y	+0.556 z	+0.0217 = 0			

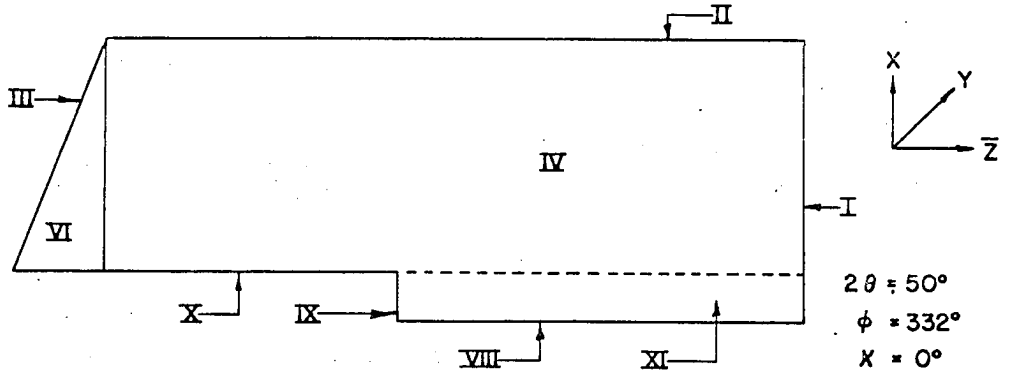

(a)

Figure 6a. Front view of single crystal

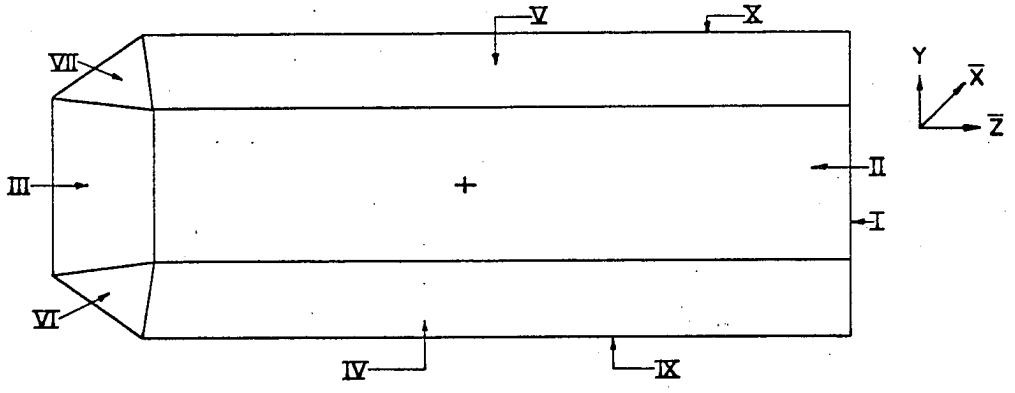

(b)

Figure 6b. Side view of single crystal

in cm.

Although the majority of the reflections appeared to be mirrored across the h axis some question arose concerning a few reflections with high order k indices. Since absence of this mirror plane would lower the symmetry to the monoclinic system, further confirmation was desired. The intensities of 34 reflections of the type $\bar{h}k\ell$ were measured and compared with the corresponding $hk\ell$ reflections. Upon application of the absorption corrections, these intensities were found identical within the statistical error so Pmmm symmetry was established.

The principal problem encountered in calculating standard deviations is involved in weighting the very weak reflections. The standard deviation of the intensity is calculated in the usual fashion (52); i.e. for some function g(x,...z),

$$\sigma_g^2 = \left[\frac{\partial g}{\partial x}\right]^2 \sigma_x^2 + \ldots + \left[\frac{\partial g}{\partial z}\right]^2 \sigma_z^2 .$$

The functional dependence of the intensities are

$$I(hk\ell) = \left[C_T(hk\ell) - C_B(hk\ell)\right] \; / \; \left[A(hk\ell)D(hk\ell)\right] ,$$

where C_T and C_B are total and background counts respectively while A and D are the absorption and decomposition corrections. Then

$$\sigma_I^2 = \frac{1}{A^2D^2} \; (C_T - C_B)^2 \left[\frac{\sigma_A^2}{A^2} + \frac{\sigma_D^2}{D^2}\right] + \sigma_{C_T}^2 + \sigma_{C_B}^2 .$$

The standard deviations of the peak and background counts are the square root of the number counted. The standard deviation of the decomposition correction was assigned a functional relationship representative of the spread of the standard curves from the average curve of Fig. 5. The standard deviation of the absorption correction was assigned the value 0.05A representative of the error present in measuring crystal dimensions and orientation. Then

$$\sigma_I = \frac{1}{AD}\left\{ (C_T - C_B)^2 \left[K_A^2 + \left(\frac{f(t)}{D}\right)^2 \right] + C_T + C_B \right\}^{\frac{1}{2}} .$$

The structure factor is defined

$$F(hk\ell) = \left[\frac{I}{LP}\right]^{\frac{1}{2}}$$

where I is the corrected intensity and L and P are Lorentz and polarization corrections (37). Use of the above procedure results in undefined standard deviations for data with zero intensity. The following formula may be derived using finite difference methods (29),

$$\sigma_F = \left[(I + \sigma_I)^{\frac{1}{2}} - I^{\frac{1}{2}}\right] \left[1/LP\right]^{\frac{1}{2}}.$$

This method assumes no error in the Lorentz and polarization corrections.

Computer programs were written applying the above corrections and the data reduced to their structure factors.

Of the 612 data points, less than 350 have appreciable intensity. Using counter data, large errors are present in the very weak reflections, consequently, a significance test was applied. All data having $F_{obs}(hk\ell) \leq 2\sigma_F$ were termed "unobserved" and were not included in the final refinements. Justification for this procedure will be given in the Refinement section.

Structure Solution and Refinement

Examination of the "sharpened" Patterson map revealed two large peaks approximately 2.5Å from the origin. This is nearly the sum of the covalent radii of niobium and bromine atoms (51) so they were used in superpositions. These superpositions were unsuccessful because of the broadness of the peaks. This leads to error in the initial vector location which is compounded in subsequent superpositions. It was decided at this time to calculate a symmetry map based on the low symmetry $Pna2_1$ space group.

$Pna2_1$ is a polar space group, i.e. there is no Z dependence in its interequivalent-point vectors. Thus, one Z-coordinate within the structure is independent of the choice of origin. This dictates Z-independence in the symmetry map. Thus the symmetry map consists of lines of constant magnitude

in the Z direction. A great deal of the map consisted of zeroes with a corresponding great simplification of the problem.

There were ridges of SM($\underline{\mu}$) = 582 for the lines (5, 10, Z), (15, 30, Z), (25, 10, Z) and 35, 30, Z) where all coordinates are expressed in 40th's of their respective lattice parameters. The next largest values of SM($\underline{\mu}$) were 280 and 273. For simplicity, Z was arbitrarily chosen as 10.0. The X and Y coordinates were estimated as 35.2 and 30.5, respectively. Superpositions of the Patterson upon the symmetry map were performed by placing the Patterson origin upon the point (35.2, 30.5, 10) and its equivalent positions and using the minimum function as previously described. The resulting electron density map contained 90 peaks of height 150 or greater with numerous smaller peaks also present.

A peak at (34.9, 1.0, 15.1) was selected for a new set of superpositions. The resulting map contained 28 unique heavy atom positions. Using 3.0$\mathring{A}$ as the maximum intramolecular niobium-bromine distance, this gave an image of discrete molecules containing one niobium and six bromine atoms. The six atoms contained several sets of four reasonable atom positions, but no unique set could be determined with cer-

tainty. All reasonable sets of bromine atoms contained one cis and one trans bromine pair. The criteria of reasonableness was agreement with the Patterson map and inter-bromine distances of 3.3Å or more.

A possible atom position (39.8, 39.0, 5.9) was selected and four more superpositions performed. The result was a single image of a cis $NbBr_4$ structure. Subsequent superpositions using the remaining bromine position retained this image. Though electron density was present in the unit cell trans to the cis bromine atoms, it was not possible to locate peaks for the carbon and nitrogen atoms. The atom positions and final peak heights are given below. This model uniquely established the space group as $Pna2_1$ since no mirror is present in the Z direction.

Atom	X/40a	y/40b	Z/40c	Peak height
Nb	35.2	30.5	10.0	155
Br(I)	34.9	1.0	15.1	130
Br(II)	34.9	20.0	5.1	134
Br(III)	39.8 —	39.0	5.9	138
Br(IV)	1.0	23.1	13.8	129

Two least squares cycles were calculated at this point varying only the scale factor. The residue was 0.23. The scattering factor tables of Hansen et al. (53) were used for

least squares and Fourier calculations.

A three dimensional Fourier electron density map was then generated. This was done by calculating the Fourier series representing the input trial structure and using the observed structure factors as the Fourier coefficients. Small changes in all atom positions were indicated on the resulting map. All cartesian coordinates were varied in three least squares cycles whereupon refinement ceased. The residue at this point was 0.19.

Since the wavelength of the molybdenum Kα radiation is just less than the bromine absorption edge, that radiation scattered by the bromine atoms experienced an anomalous phase shift. This effect is also present to a smaller degree in radiation scattered by niobium. The atomic scattering factor for such an atom may be expressed as

$$f = f_o + f' + if''$$

where f_o is a real function of $\sin\theta/\lambda$ and f' and f'' are constants giving the real and imaginary phase shift (37). The real part is included by merely subtracting f' from f_o given by scattering factor tables. The imaginary part is more difficult to apply, and because it is small, it was neglected in this investigation. The values used to correct for anomalous

dispersion were those listed by Dauben and Templeton (51).

Three least squares cycles were completed where only the cartesian coordinates were varied. The residue reduced to 0.16 with no further refinement. A new Fourier map was generated but no carbon or nitrogen atom positions were discernible.

The volume of the unit cell trans to the cis bromine atoms did however contain ridges of positive electron density, varying up to four electrons per cubic angstrom. Nitrogen atoms were placed in these volumes, 2.0Å from the niobium and a new electron density map was generated. Secondary peaks were then seen corresponding to reasonable carbon atom positions. Upon insertion of these atoms, three least squares cycles reduced the R value to 0.15. No further refinement occurred with variation of any set of variables.

A Fourier difference map was generated at this point. This map is calculated by using $[|F_{obs}| - |F_{calc}|]$ instead of F_{obs} for the Fourier coefficients. Thus if an atom which is not accounted for in the structure model is present, positive electron density is seen on the Fourier difference map, while if an atom in the model is not present in the structure, negative electron density is noted. The Fourier difference

map showed density of 2-3 electrons per cubic angstrom in chemically unreasonable volumes of the unit cell.

No other evidence of unaccounted for species within the compound was present so a "spurious peak" calculation was undertaken. Scattering positions corresponding to the spurious peaks were used for a structure factor calculation. Examination of the data showed eight structure factors were calculated with large values (30 or over). These data were removed and least squaring on the original model was resumed. A total of six least squares cycles varying cartesian coordinates of all atoms and isotropic variation of the temperature factors reduced the residue to 0.11.

Final least squares refinement was done by varying all atomic parameters for an additional eight cycles. The discrepancy index settled at 0.089 with no further reduction. An R factor summary is given in Table 3. The consistency of the residue for the various classes of reflections indicate no irregularities in the refinement. A total of 380 reflections were included in the final refinement. These are listed in Table 4. Table 5 includes all unobserved data and the spurious peak reflections, which are asterisked. All rejected data gave F_{calc} small for the final model, which indicates

Table 3. R-factor summary for $NbBr_4(CH_3CN)_2$

Class of refl.		Observed data only R	Observed data only No. refl.	All reflections R	All reflections No. refl.
All orders		0.089	380	0.135	612
H	even	0.079	228	0.128	323
H	odd	0.110	152	0.124	289
K	even	0.101	189	0.139	318
K	odd	0.079	191	0.142	294
L	even	0.086	198	0.121	288
L	odd	0.093	182	0.147	324
H+K	even	0.084	227	0.134	312
H+K	odd	0.100	153	0.135	300
H+L	even	0.089	212	0.120	336
H+L	odd	0.089	168	0.159	266
K+L	even	0.091	203	0.131	325
K+L	odd	0.086	177	0.143	287
H+K+L	even	0.082	217	0.148	320
H+K+L	odd	0.102	163	0.126	292

$$\left[\frac{\left[\left(F_{obs} - F_{calc}\right)^2 W\right]}{N_{obs} - N_{var}}\right]^{\frac{1}{2}} = 1.2796$$

Table 4. Comparison of observed and calculated structure factors for those reflections called observed in the final refinement

H	K	L	F_{obs}	F_{calc}	A	B	H	K	L	F_{obs}	F_{calc}	A	B
0	0	2	176.5	157.6	-242.8	8.6	2	3	6	47.4	52.8	-62.6	51.9
0	0	4	213.0	214.8	-330.3	23.9	2	3	7	32.6	28.6	40.4	17.6
0	0	6	62.1	58.5	81.8	-38.1	2	3	8	80.5	77.5	118.9	-11.4
0	0	8	175.6	175.7	269.5	-27.1	2	3	9	44.3	48.9	65.0	-38.3
0	0	10	136.9	145.8	-220.4	44.7	2	3	10	57.7	44.7	-64.2	-25.1
0	1	1	147.0	138.4	213.2	6.0	2	4	1	101.0	103.6	139.1	-16.8
0	1	3	98.0	96.8	-147.1	-25.2	2	4	2	37.4	44.7	-9.3	68.3
0	1	5	14.8	26.3	35.1	20.2	2	4	7	80.3	70.0	-107.8	-5.6
0	1	9	66.0	68.3	100.3	-32.0	2	4	8	29.8	36.6	-9.0	55.7
0	1	11	71.4	72.2	-109.9	17.2	2	4	9	88.6	72.5	110.6	-16.0
0	2	0	204.3	200.8	309.5	-0.0	2	5	1	56.2	59.5	91.3	-9.5
0	2	2	59.1	54.2	59.6	58.6	2	5	2	37.2	50.2	51.4	-57.8
0	2	4	271.1	279.8	-431.1	-13.5	2	5	3	28.6	31.7	31.7	10.8
0	2	6	147.0	141.3	212.2	-49.5	2	5	4	68.3	73.5	-112.8	10.9
0	2	8	38.4	55.2	83.8	15.2	2	5	5	56.6	55.8	-85.3	11.4
0	2	10	27.3	29.9	-32.9	32.3	2	6	0	37.1	33.6	-51.9	0.0
0	2	12	74.6	76.6	-119.6	-19.8	2	6	1	31.0	10.8	-0.1	-16.7
0	3	1	22.6	12.7	0.2	-19.6	2	6	3	52.0	47.7	72.1	14.1
0	3	3	51.5	47.2	72.7	-4.8							
0	3	5	139.5	130.5	-195.6	47.2	3	1	2	276.0	272.0	16.4	419.1
0	3	7	112.1	105.0	161.2	-14.7	3	1	3	70.6	70.0	4.2	-107.8
0	3	9	31.9	39.8	-29.2	-53.9	3	1	4	67.4	69.2	-44.9	-96.7
0	4	0	123.1	128.6	198.3	-0.0	3	1	5	28.7	23.5	-9.3	-35.0
0	4	2	85.8	88.3	-78.3	111.4	3	1	6	159.2	159.4	-10.2	-244.6
0	4	4	52.7	50.4	-57.5	-52.2	3	1	7	49.7	41.5	-8.6	63.4
0	4	6	47.6	51.1	-50.7	-60.2	3	1	8	93.9	92.3	39.4	136.7
0	4	8	111.0	114.1	165.1	60.9	3	1	10	58.2	64.8	5.6	99.8
0	4	10	55.0	43.9	-65.8	15.4	3	1	11	29.7	23.1	-16.7	-31.4
0	5	1	66.0	68.5	87.5	-59.2	3	2	0	20.5	20.8	-32.1	0.0
0	5	3	61.8	61.2	-69.7	63.5	3	2	1	19.5	18.8	-25.3	-14.0
0	5	5	28.3	27.8	10.7	41.5	3	2	3	61.5	57.1	41.4	77.7
0	6	2	61.0	69.4	53.3	92.8	3	2	4	26.1	17.4	-16.4	-21.1
0	6	4	30.4	46.7	-61.0	-38.3	3	2	5	30.3	25.7	-1.5	-19.6
1	1	1	52.8	49.3	23.5	72.2	3	2	7	51.0	45.9	-34.1	-62.1
1	1	3	52.7	60.4	-14.8	-91.9	3	2	9	46.8	42.7	9.9	67.1
1	1	4	84.0	86.0	-6.8	-132.4	3	2	11	30.4	32.9	50.3	6.8
1	1	5	52.1	60.1	-5.2	-92.6	3	2	12	31.7	14.2	-21.4	-4.8
1	1	6	20.8	17.3	-20.6	16.8	3	3	0	60.6	65.4	100.8	0.0
1	1	7	68.8	64.9	-4.3	100.0	3	3	1	22.5	36.2	-37.6	41.2
1	1	8	80.1	85.8	45.2	124.3	3	3	2	137.8	140.7	-35.2	211.1
1	1	9	43.5	44.8	8.2	68.6	3	3	4	39.8	44.6	-48.6	-48.7
1	1	10	50.3	55.9	-14.8	-85.0	3	3	5	35.5	27.8	-21.4	-37.2
1	1	11	50.1	48.2	-12.0	-73.4	3	3	6	103.0	103.4	19.7	-158.2
1	2	0	17.1	10.9	16.7	0.0	3	3	8	28.1	51.6	50.8	61.1
1	2	1	85.1	84.2	-36.7	-124.5	3	3	10	69.6	64.6	-47.0	87.8
1	2	2	46.9	40.5	18.9	-59.6	3	4	5	27.3	28.2	-9.1	-42.5
1	2	3	99.5	104.1	-34.6	156.7	3	4	6	28.2	24.9	-35.6	14.1
1	2	5	21.1	48.7	74.5	9.8	3	4	9	68.1	62.2	58.0	76.4
1	2	6	21.9	28.4	11.4	42.2	3	5	1	28.6	11.3	12.7	11.9
1	2	7	71.2	73.2	-45.5	-103.3	3	5	2	30.4	35.5	-4.7	54.6
1	2	9	47.2	35.6	-6.2	54.5	3	5	4	71.0	63.2	-97.4	4.1
1	2	11	29.0	24.2	17.3	33.1	3	5	5	30.3	32.9	46.8	-19.3
1	3	0	20.6	24.5	37.7	0.0	3	5	6	74.3	63.7	75.4	-62.9
1	3	1	57.1	57.2	-26.2	84.1	3	6	3	34.9	44.2	67.4	9.8
1	3	3	65.4	54.3	14.1	-82.5	4	0	0	42.3	41.2	-63.5	0.0
1	3	4	39.8	51.9	-75.0	-28.0	4	0	1	56.4	55.8	-82.5	-24.4
1	3	5	42.8	44.6	-22.4	-65.0	4	0	3	67.3	61.5	-80.3	50.4
1	3	6	45.3	48.6	63.3	40.2	4	0	4	77.8	77.7	-118.8	14.4
1	3	7	41.2	49.0	30.1	69.3	4	0	5	81.1	87.0	134.0	4.2
1	3	10	42.9	32.8	-22.8	-45.2	4	0	6	154.4	159.2	244.0	-26.4
1	4	0	45.6	42.8	66.0	0.0	4	0	8	101.4	104.6	-161.2	-3.8
1	4	1	75.2	83.2	-62.0	-112.4	4	0	9	30.6	27.4	-39.3	15.4
1	4	3	105.7	100.2	18.8	153.4	4	0	10	28.6	32.5	-23.5	44.2
1	4	5	25.9	10.6	-0.4	16.3	4	0	11	30.1	21.7	-31.4	11.7
1	4	7	71.7	72.9	11.8	-111.8	4	1	0	18.3	5.9	-9.1	-0.0
1	5	0	56.8	62.2	95.9	-0.0	4	1	1	18.5	22.0	-18.6	28.3
1	5	2	55.2	58.4	-58.6	-68.4	4	1	2	35.1	14.9	21.6	-7.9
1	5	3	27.5	40.2	-39.4	-67.8	4	1	3	100.1	105.5	157.0	-42.7
1	5	5	28.7	32.2	38.3	-31.7	4	1	4	24.5	15.3	-22.4	7.3
1	5	6	52.8	34.4	34.7	40.2	4	1	5	118.0	116.1	-178.9	3.9
1	6	1	41.8	48.9	48.1	-58.1	4	1	6	23.6	22.5	34.6	-7.3
2	0	0	71.9	67.4	103.9	-0.0	4	1	7	71.6	68.6	102.1	27.8
2	0	1	201.8	200.5	309.0	-8.5	4	1	8	26.2	25.4	-36.4	-14.4
2	0	2	52.2	53.4	-81.5	11.4	4	1	9	27.5	24.8	-34.8	-15.9
2	0	4	43.7	40.6	-53.6	32.3	4	2	0	70.1	70.9	109.3	-0.0
2	0	5	19.8	33.3	-50.4	-9.5	4	2	1	62.8	64.2	-98.3	-10.6
2	0	6	83.4	80.7	119.8	-33.6	4	2	2	101.7	98.4	-146.6	39.0
2	0	7	123.8	124.9	-192.3	-10.1	4	2	4	83.7	77.2	118.5	-11.8
2	0	9	121.3	121.1	186.5	9.7	4	2	5	30.9	31.1	48.0	0.5
2	0	10	78.5	81.3	-117.1	44.9	4	2	7	26.1	35.8	51.9	-18.7
2	0	12	48.0	50.5	76.5	-15.0	4	2	8	27.2	13.0	1.1	20.1
2	1	0	80.2	83.8	-129.2	0.0	4	2	9	69.1	39.2	-60.0	7.0
2	1	1	44.6	49.1	73.5	18.1	4	2	10	75.9	75.9	-114.7	23.2
2	1	2	83.2	82.3	121.8	-35.5	4	3	5	63.9	51.8	-79.8	-3.0
2	1	3	17.5	21.4	13.7	-30.1	4	2	7	27.6	39.6	-44.8	41.5
2	1	4	96.8	93.4	-143.8	5.2	4	3	8	28.8	18.1	-20.8	-18.6
2	1	6	78.0	73.5	110.6	24.4	4	3	9	82.1	90.5	138.1	-20.0
2	1	7	23.5	10.5	5.8	15.2	4	4	0	95.4	89.5	-138.0	0.0
2	1	8	42.3	37.9	-58.4	-3.0	4	4	2	53.8	63.9	76.4	62.2
2	1	10	44.7	43.3	65.9	-10.1	4	4	5	28.1	20.5	31.4	-3.2
2	2	0	25.6	28.0	43.2	-0.0	4	4	6	42.7	32.3	42.4	-26.1
2	2	2	35.8	30.9	-27.6	38.9	4	4	7	29.9	34.8	21.4	7.6
2	2	3	142.7	144.0	221.7	10.4	4	4	8	73.4	71.5	-96.0	54.2
2	2	4	21.0	31.4	-48.3	-2.5	4	5	3	84.6	73.2	112.3	-11.4
2	2	5	142.8	145.5	-224.2	3.1	4	5	4	30.2	17.1	26.4	0.8
2	2	6	72.4	65.9	95.0	-36.0	4	5	5	103.2	104.7	-160.8	-13.1
2	2	8	27.8	18.6	-23.0	17.2	5	1	1	82.6	86.7	20.6	-132.1
2	2	9	27.3	13.9	21.4	1.2	5	1	2	116.2	123.5	22.2	189.0
2	2	10	31.3	44.2	-62.5	27.2	5	1	3	96.9	96.8	11.1	148.8
2	2	11	55.1	72.4	111.5	4.0	5	1	4	75.5	79.8	-30.6	-119.2
2	3	0	89.2	94.2	145.2	-0.0	5	1	5	69.2	73.4	-30.6	108.9
2	3	1	71.7	69.2	104.5	21.6	5	1	6	55.4	49.6	0.7	-76.4
2	3	2	77.0	79.3	-102.5	-66.5	5	1	7	71.8	77.1	21.3	-116.9
2	3	3	38.7	46.8	60.4	-39.5	5	1	8	77.1	77.9	20.6	118.4
2	3	5	89.9	84.5	-129.7	23.8	5	1	9	45.4	56.5	12.7	-86.2

Table 4. (Continued)

H	K	L	Fobs	Fcalc	A	B
[illegible]	1	11	[illegible]	[illegible]	[illegible]	81.1
[illegible]	[illegible]	0	32.8	[illegible]	-35.8	0.0
[illegible]	[illegible]	1	53.1	58.1	-52.8	-72.4
[illegible]	[illegible]	2	32.7	23.7	[illegible]	39.5
[illegible]	[illegible]	3	75.9	78.5	23.1	118.8
[illegible]	[illegible]	[illegible]	48.1	58.9	-17.8	-73.2
[illegible]	[illegible]	8	33.9	18.3	-20.3	19.6
[illegible]	3	1	68.2	73.2	27.3	-109.5
[illegible]	3	2	34.8	30.7	-47.6	62.0
[illegible]	3	3	65.3	70.9	-2.2	109.2
[illegible]	3	[illegible]	46.7	54.6	3.1	84.1
[illegible]	[illegible]	[illegible]	28.2	27.8	15.3	-40.0
[illegible]	3	[illegible]	63.0	60.6	-19.0	-91.5
[illegible]	[illegible]	0	52.3	58.0	-89.4	0.0
[illegible]	[illegible]	1	52.6	48.0	35.4	-65.1
[illegible]	[illegible]	2	44.7	43.9	28.1	61.6
[illegible]	[illegible]	3	69.8	68.8	-16.3	104.8
[illegible]	[illegible]	4	44.3	33.2	49.3	-13.9
[illegible]	[illegible]	6	47.6	35.7	-10.0	-54.2
[illegible]	5	2	30.1	12.8	5.5	-18.9
[illegible]	5	3	41.1	47.4	30.6	66.4
[illegible]	[illegible]	5	39.1	29.4	-17.3	41.9
6	0	0	189.1	188.1	290.0	-0.0
6	0	1	119.6	127.5	-193.3	-35.8
6	0	3	38.1	31.5	17.3	45.3
6	0	4	180.5	181.0	-278.5	16.7
6	0	6	96.8	101.1	152.4	-32.5
6	0	7	87.5	88.4	133.0	-29.5
6	0	8	64.1	55.9	84.1	-18.6
6	0	9	90.0	92.9	-142.3	17.2
6	0	10	64.2	62.8	-88.9	38.4
6	2	0	61.5	60.4	93.1	-0.0
6	1	1	24.5	5.1	-7.1	-3.4
6	1	2	53.5	60.2	-92.8	-1.2
6	1	4	62.0	63.1	96.3	13.7
6	1	5	37.1	48.8	-73.1	18.0
6	1	6	43.6	52.0	-80.2	-2.6
6	1	7	37.7	36.4	56.0	3.3
6	1	8	28.4	40.5	60.6	-15.2
6	1	10	31.1	42.7	-65.2	8.9
6	2	0	175.1	172.8	266.4	-0.0
6	2	1	23.9	12.6	13.0	-14.4
6	2	2	51.5	50.1	-68.3	36.1
6	2	3	100.7	100.0	-152.4	22.6
6	2	4	95.0	101.6	-156.6	-4.1
6	2	5	100.5	97.4	150.1	-2.5
6	2	6	42.3	44.5	57.6	-37.4
6	2	7	28.2	15.9	-20.2	-13.9
6	2	8	69.5	78.9	121.1	10.7
6	2	9	30.7	5.9	1.6	8.9
6	2	10	58.5	63.9	-95.6	23.7
6	3	0	66.6	63.7	-98.3	0.0
6	3	1	57.9	53.9	80.8	-19.1
6	3	2	42.2	49.6	76.4	0.2
6	3	4	30.8	33.9	-46.8	23.3
6	3	5	33.2	41.5	-49.1	41.0
6	3	6	51.2	43.1	65.2	-13.0
6	3	8	50.2	52.9	-78.2	-23.0
6	4	0	50.1	40.5	62.4	-0.0
6	4	1	62.0	64.6	-98.3	16.4
6	4	2	32.6	48.2	13.2	73.1
6	4	4	67.8	68.8	-100.2	-35.1
6	4	6	31.1	32.2	31.9	-38.1
6	5	2	37.7	30.5	-44.1	16.3
6	5	4	36.1	51.7	79.5	6.5
6	5	5	34.1	38.7	-49.3	33.7
7	1	0	23.9	21.3	32.8	0.0
7	1	1	24.0	29.7	29.2	35.4
7	1	3	26.4	35.3	23.3	-49.2
7	1	4	51.5	48.6	-30.8	-68.3
7	1	5	45.7	40.3	-59.7	-17.3
7	1	6	35.0	34.3	-2.1	52.8
7	1	7	38.3	26.4	18.5	36.3
7	1	8	59.1	58.0	43.6	78.1
7	1	9	30.9	13.6	20.9	2.0
7	1	10	71.6	58.5	-18.3	-88.3
7	2	1	57.6	60.8	-37.5	-85.9
7	2	2	29.1	14.5	-13.2	18.0
7	2	3	77.1	66.8	-21.7	100.6
7	2	4	30.3	30.5	45.6	-11.6
7	2	5	33.8	36.0	48.3	27.5
7	2	6	45.3	26.1	-40.2	-0.3
7	2	7	57.2	52.9	-17.8	-79.6
7	3	1	27.4	24.7	35.3	14.4
7	3	3	39.8	16.1	-22.1	-11.4
7	3	6	57.2	45.1	37.2	58.8
7	3	9	36.2	20.4	26.9	16.2
7	4	0	52.2	40.0	-61.7	0.0
7	4	1	72.5	70.4	-47.1	-97.7
7	4	3	82.1	80.8	-9.1	124.3
7	4	7	67.6	65.0	9.0	-99.8
7	5	0	55.1	35.8	55.2	0.0
8	0	0	212.2	197.6	304.6	-0.0
8	0	2	73.8	84.1	-129.3	10.3
8	0	3	90.6	86.6	126.9	41.7
8	0	4	57.9	61.2	-93.5	11.8
8	0	4	49.4	61.2	-93.5	11.8
8	0	5	65.5	72.6	-111.9	-5.7
8	0	7	63.5	46.0	-63.4	-31.8
8	0	8	81.1	83.6	128.8	-0.6
8	0	10	89.7	90.2	-136.8	25.6
8	1	0	53.6	50.5	77.9	-0.0
8	1	1	86.4	73.8	113.7	5.0
8	1	2	27.5	43.7	-55.5	-38.1
8	1	3	57.0	46.7	-71.5	-8.5
8	1	4	28.6	12.4	8.2	17.3
8	1	6	28.3	16.2	-10.1	22.9
8	1	10	36.4	24.4	-37.0	-6.8
8	2	0	58.5	55.1	84.9	-0.0
8	2	1	72.7	78.0	119.0	-16.8
8	2	3	34.2	33.1	46.9	20.2
8	2	4	114.9	124.9	-192.4	-7.9
8	2	5	46.9	31.5	-48.5	3.9
8	2	6	72.8	86.2	130.3	-26.0
8	2	7	80.5	65.3	-98.9	-18.5
8	2	9	54.4	61.0	93.5	9.7
8	3	3	44.3	45.9	70.8	-3.0
8	3	4	50.5	57.9	-85.2	26.6
8	3	5	81.4	84.0	-126.6	27.1
8	3	6	62.3	50.9	59.9	50.8
8	3	7	61.6	59.4	90.8	-11.3
8	3	8	35.8	21.8	5.1	-33.2
8	4	0	60.0	64.7	99.7	-0.0
8	4	2	53.6	51.1	-54.1	57.3
8	4	3	55.0	54.1	83.3	-4.7
8	4	5	60.5	63.0	-96.3	12.5
8	5	0	61.4	43.2	66.6	0.0
8	5	1	50.0	56.1	81.4	-29.1
9	1	1	59.6	63.0	48.1	84.3
9	1	2	108.6	115.8	-8.9	178.3
9	1	3	63.4	67.9	19.2	-102.8
9	1	4	63.3	48.7	-6.0	-74.9
9	1	5	40.5	43.9	-45.4	-50.1
9	1	6	64.6	62.7	-13.3	-95.8
9	1	7	67.2	54.9	6.7	84.3
9	1	8	56.4	61.9	31.3	90.2
9	2	3	40.6	42.4	-4.8	65.2
9	2	7	33.7	38.0	-38.8	-43.8
9	2	8	39.0	13.9	11.5	18.1
9	3	1	46.3	33.2	-2.1	51.1
9	3	2	62.3	59.3	14.4	90.3
9	3	3	48.7	31.6	5.1	-48.4
9	3	5	42.3	30.2	-9.6	-45.6
9	3	6	51.7	49.6	43.8	-62.7
9	4	3	44.2	50.0	48.3	60.0
10	0	0	33.3	21.6	33.4	0.0
10	0	4	40.8	46.4	71.4	3.7
10	0	5	34.5	42.5	64.9	-9.6
10	0	6	40.9	37.9	41.8	-40.8
10	0	7	53.0	50.7	-66.1	-41.7
10	0	8	46.0	26.3	-39.5	9.5
10	1	1	62.2	58.6	89.4	13.5
10	1	4	55.5	45.5	-69.0	12.1
10	1	6	54.8	41.9	63.6	11.6
10	2	0	36.0	42.0	-64.8	-0.0
10	2	3	42.3	45.1	63.8	27.8
10	2	6	42.5	55.6	78.8	-13.7
10	3	1	35.4	45.0	65.1	23.9
10	3	2	35.6	49.0	-56.6	-52.2
10	3	3	54.9	55.2	79.1	-31.6
10	3	5	70.9	79.6	-122.7	-3.1
11	1	4	35.5	35.6	-14.4	-52.9
11	1	6	66.8	70.1	1.9	-108.0
11	2	0	35.2	44.6	-68.8	0.0
11	2	1	35.3	9.5	2.0	-14.5
11	2	2	35.6	30.9	30.6	36.6
12	0	0	35.7	32.0	49.3	-0.0
12	0	3	67.8	73.9	-96.3	60.9
12	0	4	74.4	77.7	-119.7	1.7
12	0	5	75.7	80.1	123.0	12.1
12	2	0	72.8	77.5	119.5	-0.0

Table 5. Comparison of observed and calculated structure factors for those reflections called unobserved in the final refinement

H	K	L	F_{obs}	F_{calc}	A	B	H	K	L	F_{obs}	F_{calc}	A	B
0	0	12	29.2	6.3	8.0	-5.6	5	2	10	30.5	17.6	11.7	24.5
0	1	7	10.6	10.0	-5.9	9.5	5	2	11	31.9	32.2	46.4	17.9
0	1	11	30.1	35.3	-36.0	20.8	5	3	0	24.4	60.2	92.8	-0.0
0	1	7	29.8	37.5	11.9	-56.6	5	3	4	48.5	24.2	-21.7	-30.3
0	2	0	13.7	22.8	-15.2	0.0	5	3	8	29.5	39.3	42.3	43.4
							5	3	9	30.7	34.1	15.3	-50.1
1	1	0	55.2	14.7	22.6	-0.0	5	3	10	32.0	36.2	-55.3	7.5
1	1	12	29.6	43.9	-31.1	-60.1	5	4	5	30.5	17.1	23.5	-12.1
1	2	4	19.9	43.7	-56.8	36.1	5	4	7	83.9	61.1	-52.7	-78.1
1	2	8	2.4	11.1	13.4	-10.8	5	4	8	32.2	34.4	-51.4	13.4
1	3	10	27.5	17.2	14.2	-22.3	5	5	0	72.5	25.5	39.2	-0.0
1	3	12	30.1	14.9	-22.5	-4.4	5	5	1	30.4	42.7	-10.1	-65.1
1	4	2	46.8	15.9	9.8	-22.5	5	5	4	55.7	54.7	-81.8	20.5
1	4	8	26.5	20.3	-2.4	31.3	5	5	4	26.9	54.7	-81.8	20.5
1	4	9	27.8	28.0	-16.8	19.7	5	5	6	34.2	51.8	81.0	-0.5
1	5	11	30.4	31.5	5.9	-48.2							
1	5	2	24.3	47.6	-25.6	-68.8	6	0	2	36.1	10.2	-11.4	8.4
1	5	4	41.6	15.2	-12.5	15.6	6	0	5	24.7	6.2	8.5	4.3
1	5	6	26.7	37.4	-24.3	52.2	6	0	11	32.2	20.8	30.6	9.5
1	5	9	29.8	29.9	-25.4	38.5	6	1	3	45.8	19.5	27.8	-11.4
1	5	10	31.0	27.0	-16.8	-38.0	6	1	9	29.7	16.5	-6.6	-24.6
1	6	1	24.9	31.3	10.2	50.3	6	1	11	32.5	33.2	-13.7	1.1
1	6	4	20.1	22.9	-14.2	32.4	6	3	3	16.6	23.3	-35.9	-7.7
1	6	7	30.2	21.8	-8.1	32.7	6	3	7	29.9	25.8	37.5	-11.2
1	6	0	30.1	7.1	11.0	-0.0	6	3	9	32.2	40.2	46.6	-40.7
1	6	2	30.3	38.6	23.4	-54.7	6	4	3	52.7	16.8	18.7	-18.0
1	6	3	93.8	51.9	-25.6	75.9	6	4	5	48.4	15.9	-23.6	-6.7
1	6	4	31.9	37.0	-57.0	0.2	6	4	7	86.3	52.3	80.0	10.6
							6	4	8	33.1	43.5	50.8	43.8
2	0	3	48.8	12.8	-18.2	7.6	6	5	0	31.3	3.7	5.7	0.0
2	0	8	24.6	6.3	1.3	-9.7	6	5	1	31.4	28.6	11.6	-42.6
2	0	11	29.0	4.7	1.6	7.1							
2	1	5	16.1	31.1	-45.7	14.7	7	1	2	24.4	19.4	1.0	-30.0
2	1	9	16.7	32.8	44.7	-23.7	7	2	0	52.9	13.8	-21.3	0.0
2	1	11	70.9	26.1	-40.2	2.4	7	2	8	30.6	15.5	12.8	20.2
2	1	12	30.9	45.2	-69.6	4.4	7	2	9	27.9	17.5	-13.1	23.6
2	2	1	43.7	15.9	21.1	-12.5	7	2	10	33.2	10.9	9.1	-14.0
2	2	7	24.8	5.1	0.7	-7.8	7	3	0	47.0	27.9	43.1	-0.0
2	2	12	31.7	31.8	41.2	-26.4	7	3	2	28.8	30.7	-2.9	-47.2
2	3	4	51.6	17.6	24.4	12.1	7	3	4	71.9	35.3	-50.3	-20.6
2	3	11	31.6	36.7	-55.2	12.2	7	3	5	58.6	13.7	16.1	-13.8
2	4	0	25.0	4.6	-7.1	0.0	7	3	7	32.5	14.5	-21.6	5.8
2	4	3	25.7	10.4	9.8	12.6	7	3	8	36.4	17.3	11.8	23.9
2	4	4	26.9	34.2	25.9	-45.8	7	4	2	31.4	24.2	37.3	1.9
2	4	5	26.9	12.2	-10.1	15.9	7	4	4	46.2	7.7	-8.5	-8.4
2	4	6	27.7	21.6	-4.5	-33.0	7	4	5	34.3	25.6	21.4	33.1
2	5	0	27.9	7.8	12.0	0.0	7	4	6	33.8	8.9	8.1	11.1
2	5	6	68.7	44.5	51.5	45.3	7	5	1	34.1	29.7	-45.7	-1.3
2	5	7	31.3	13.1	9.8	-17.7	7	5	2	87.2	44.0	-31.5	-60.1
2	6	2	31.4	32.3	19.1	45.9	7	5	3	33.0	19.2	26.7	12.8
							7	5	4	58.2	16.2	-17.3	17.9
3	1	0	28.0	5.7	8.8	-0.0							
3	1	1	273.5	62.5	37.6	88.7	8	0	1	26.6	26.0	26.6	-30.1
3	1	9	26.8	16.7	18.7	17.7	8	0	6	54.8	24.1	33.0	-17.1
3	1	12	83.8	65.4	-37.4	-93.6	8	0	9	33.4	33.3	45.4	24.0
3	2	2	51.1	26.9	31.7	26.7	8	1	5	29.4	22.5	33.1	10.6
3	2	6	24.1	6.7	1.6	10.2	8	1	7	60.0	26.7	-41.1	1.2
3	2	8	26.5	11.1	-12.4	11.9	8	1	8	32.7	28.6	41.0	-16.4
3	2	10	29.2	20.3	26.3	-17.0	8	1	9	34.0	48.3	71.7	-19.9
3	3	3	17.7	28.5	24.9	-36.2	8	2	2	28.9	31.7	39.2	29.1
3	3	7	26.9	25.5	22.9	31.9	8	2	8	34.0	13.3	5.8	19.7
3	3	9	61.7	19.4	-20.6	21.6	8	3	0	60.4	25.3	39.0	0.0
3	3	11	32.0	16.7	16.1	-20.1	8	3	1	30.6	3.1	2.6	-3.9
3	4	0	25.5	23.8	36.6	-0.0	8	3	2	30.9	46.7	9.1	-71.3
3	4	1	25.5	35.3	51.5	-17.3	8	4	1	33.3	37.0	57.0	-1.3
3	4	2	52.8	19.0	-28.9	-4.7	8	4	6	36.1	28.9	-32.1	-30.9
3	4	3	26.7	44.7	25.8	63.9							
3	4	4	26.7	17.2	25.3	-7.7	9	1	0	59.0	10.7	16.5	0.0
3	4	7	86.0	53.3	-65.1	-50.1	9	1	9	36.4	25.0	29.0	25.4
3	4	8	30.2	21.6	32.2	8.5	9	2	0	51.8	7.2	-11.2	-0.0
3	5	0	28.4	54.8	84.5	-0.0	9	2	1	30.9	20.6	12.7	-29.1
3	5	3	18.0	28.3	-43.4	-4.4	9	2	2	31.2	11.7	17.9	-2.9
3	5	7	31.9	15.5	-23.4	4.9	9	2	4	30.8	10.0	-3.1	-15.2
3	6	0	31.7	9.7	-14.9	-0.0	9	2	5	59.2	23.0	27.0	-22.9
3	6	1	31.8	32.7	50.3	3.7	9	2	6	254.1	22.6	-27.4	21.5
3	6	2	29.1	23.6	27.6	-23.7	9	3	0	33.0	11.5	17.7	0.0
							9	3	4	34.4	40.8	-56.0	-28.5
4	0	2	49.9	19.3	29.7	3.1	9	4	0	33.2	8.9	13.7	-0.0
4	0	7	26.6	25.7	5.8	-39.1	9	4	1	33.3	19.7	-13.0	-27.4
4	0	12	426.0	38.7	57.8	-14.7	9	4	2	33.6	21.2	4.2	-32.4
4	1	10	29.0	7.6	8.0	8.6	9	4	4	34.5	7.8	-8.3	-8.6
4	1	11	30.4	20.4	31.0	-4.9							
4	1	12	32.0	3.9	0.8	6.0	10	0	1	31.7	43.4	62.4	-24.3
4	2	3	48.2	23.0	-27.8	22.1	10	0	2	32.0	59.2	-84.0	35.5
4	2	6	25.0	19.5	-3.1	-29.9	10	0	3	86.1	50.0	-57.1	51.9
4	2	11	31.3	8.5	-8.6	9.9	10	1	0	32.2	31.8	-49.1	0.0
4	3	0	41.5	14.4	22.2	0.0	10	1	2	32.7	42.6	58.9	-29.1
4	3	2	22.0	17.9	-27.3	-3.8	10	1	3	33.2	17.4	-17.7	-20.2
4	3	3	24.4	39.3	-1.1	-60.3	10	1	5	59.5	4.7	-6.7	2.7
4	3	4	51.5	25.6	37.9	10.8	10	1	7	34.1	18.2	-25.5	11.5
4	3	6	62.2	6.5	-0.4	-10.1	10	1	8	35.9	30.5	-44.6	-15.0
4	2	10	31.3	17.0	-21.5	15.0	10	2	1	33.6	34.1	-50.4	-14.8
4	4	1	41.2	7.8	-8.3	8.7	10	2	2	33.9	29.7	13.6	43.7
4	4	3	16.2	33.8	-50.3	-13.5	10	2	4	34.9	7.7	4.3	-11.0
4	4	9	32.0	7.5	-11.5	0.5	10	2	5	65.7	37.2	-57.3	-2.6
4	5	0	61.5	31.6	-48.7	0.0	10	2	7	37.5	29.3	37.5	-25.1
4	5	1	29.1	42.5	63.7	15.6	10	3	0	89.7	48.0	74.0	-0.0
4	5	2	70.3	12.2	11.3	15.0	10	3	4	34.1	23.4	29.5	20.7
4	5	6	31.6	11.2	8.7	-14.9	10	4	0	30.0	15.6	-24.0	0.0
4	5	7	30.7	22.9	35.3	1.6	10	4	1	37.7	39.9	61.5	1.3
4	6	0	32.2	22.5	-34.7	-0.0	10	4	2	35.4	30.9	-22.6	41.9
4	6	1	32.3	12.8	-13.5	14.5							
							11	1	0	34.2	7.6	11.8	0.0
5	1	0	28.3	2.7	4.2	0.0	11	1	1	34.2	39.2	41.8	-43.5
5	1	10	29.6	7.8	-1.8	-11.9	11	1	2	80.5	106.1	3.0	163.5
5	2	5	26.8	16.4	4.2	-24.9	11	1	3	34.9	28.6	4.0	43.8
5	2	6	28.5	36.6	-31.8	-46.8	11	1	5	30.9	34.3	-23.9	47.1
							11	1	7	35.5	26.6	6.5	-40.6

Table 5. (Continued)

H	K	L	F_{obs}	F_{calc}	A	B
11	2	3	33.6	24.2	14.7	34.3
11	2	4	54.6	21.4	27.8	-17.8
11	2	5	48.9	11.9	-7.4	-16.8
11	2	6	35.5	19.7	-15.4	-26.1
11	3	0	36.9	22.8	35.1	-0.0
11	3	1	37.0	32.9	-16.4	-47.9
11	3	2	93.0	63.4	-10.7	97.1
11	3	3	37.6	37.4	25.0	51.9
12	0	1	83.9	40.2	-43.2	-44.5
12	0	2	33.6	16.8	24.5	8.4
12	1	0	36.0	24.5	-37.7	0.0
12	1	1	36.1	19.0	-29.3	0.6
12	1	2	36.3	22.9	34.7	-6.5
12	1	3	36.7	33.6	51.4	-6.9
12	1	4	82.2	23.6	-34.1	12.4
12	1	5	30.8	42.3	-64.9	6.6
12	2	1	37.1	65.5	-97.6	-26.0
12	2	2	37.3	41.8	-61.6	18.7
12	2	3	37.7	24.5	-11.9	35.9
13	1	1	37.9	21.2	26.5	-19.2

the validity of the significance test. Errors in the spurious peak data may be due to gross fluctuations in the power supply, inaccurate angle settings or error in recording the numbers. In any case, the structure parameters are so overdetermined that exclusion of a small set of data points should not materially affect the final structure.

The weighting scheme was further analyzed at this point. An excellent weighting scheme would not be dependent on any variable of the experiment. Cruickshank and Pilling (54) proposed a method of examining this behavior. A plot is made of $\omega [|F_{obs}| - |F_{calc}|]^2$ versus an experimental variable. A perfect weighting scheme, using the correct structure, gives a straight line with zero slope. Figures 7a, b, and c are plots using $\sin\theta$, time and F_{obs} as the abscissa. These plots were prepared with groups of 25 reflections and all give reasonable deviation. The plot versus $\sin\theta$ was prepared to check the overall validity of the weighting scheme. The plot versus time was generated to examine the decomposition correction, and the structure facots plot checks against a secondary extinction problem. The latter would be evidenced by more positive values for the ordinate in the area of very large value of F_{obs}.

Figure 7a. $\omega\,[|F_o|-|F_c|]^2$ versus time

7b. $\omega\,[|F_o|-|F_c|]^2$ versus $\sin\theta/2$

7c. $\omega\,[|F_o|-|F_c|]^2$ versus F(observed)

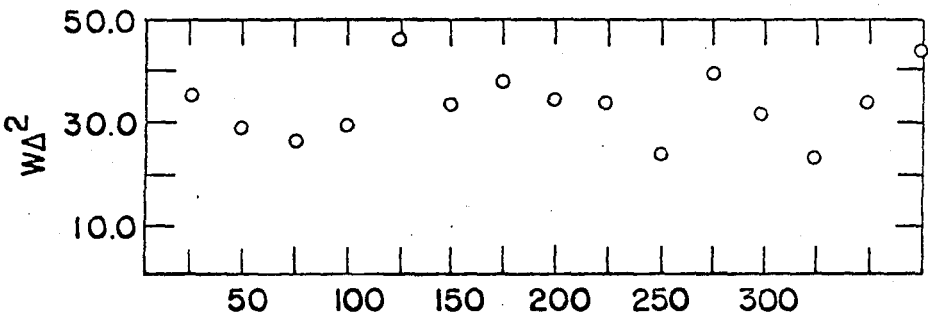
50.0
30.0
10.0
$W\Delta^2$
50
100
150
200
250
300

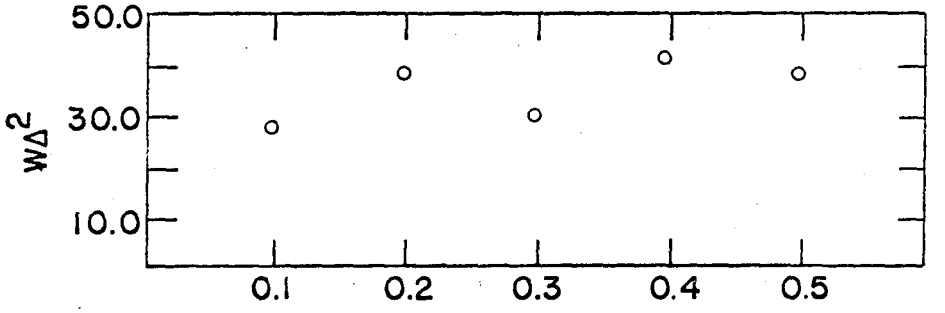
50.0
30.0
10.0
$W\Delta^2$
0.1
0.2
0.3
0.4
0.5

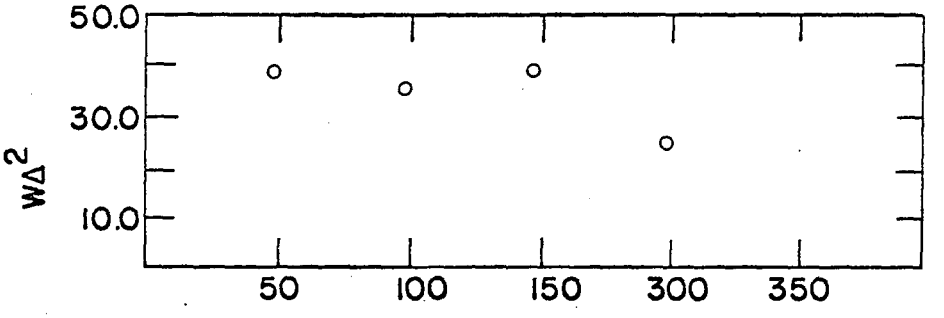
50.0
30.0
10.0
$W\Delta^2$
50
100
150
300
350

Table 6 is a listing of the atoms, the final parameters and their errors. The carbon and nitrogen atom temperature factors were varied only isotropically so only the diagonal elements are given. The anisotropic temperature factors are of the form

$$\exp\left[-h^2B_{11}+k^2B_{22}+\ell^2B_{33}+2hkB_{12}+2h\ell B_{13}+2k\ell B_{23})\right].$$

Figure 8 shows the final molecular configuration with some bond distances and angles. Table 7 lists the intramolecular distance and probable errors of all distances less than 4.0Å. Table 8 lists the interatomic angles of interest and their probable errors. All errors were calculated using the complete variance-covariance matrix and the program of Busing and Levy (35).

Figure 9 is a three-dimensional representation of the unit cell viewed from the $\{120\}$ direction. The three-dimensional effect is obtained by placing the center of a stereoscopic viewer 6.0 inches directly above the vertical line between the left and right eye views. The atoms are represented as 50% probability thermal ellipsoids. The image of the unit cell was drawn by the Symplotter assembly on the IBM 1401 computer using the program of Johnson (36).

The average Nb-Br bond distance found in this structure

Table 6. Final parameters, temperature factors and their errors for $NbBr_4(CH_3CN)_2$

Atom	x/a	y/b	z/c	B_{11}	B_{22}	B_{33}	B_{12}	B_{13}	B_{23}
Nb_1	0.88431	0.77004	0.25000	0.00181	0.01070	0.00229	-0.00044	-0.00020	-0.00066
	49	204	--	49	291	42	16	100	121
Br_1	0.85212	1.03795	0.37210	0.00214	0.00886	0.00306	0.00059	0.00013	0.00068
	117	148	182	101	293	106	154	89	136
Br_2	0.85247	0.49559	0.12756	0.00462	0.01639	0.00316	0.00106	0.00026	-0.00051
	136	174	188	115	296	107	107	110	183
Br_3	0.99626	0.96492	0.14608	0.00261	0.00904	0.00342	-0.00023	0.00030	0.00024
	92	151	167	94	279	83	158	81	151
Br_4	1.01005	0.58242	0.34286	0.00319	0.01149	0.00236	-0.00087	0.00048	0.00053
	92	147	156	103	291	82	169	77	141
N_3	0.78775	0.60508	0.33304	0.00130	0.00067	0.00073	-------	-------	-------
	903	1360	937	12	7	5			
N_4	0.78379	0.92099	0.17566	0.00151	0.00077	0.00091	-------	-------	-------
	963	757	854	14	8	6			
C_{31}	0.74068	0.54310	0.37984	0.00200	0.00098	0.000126	-------	-------	-------
	1078	1860	1228	26	8	8			
C_{32}	0.66468	0.41150	0.44402	0.00211	0.00103	0.000129	-------	-------	-------
	850	847	850	28	9	8			
C_{41}	0.72085	0.99632	0.12947	0.00193	0.00096	0.000122	-------	-------	-------
	1042	1892	1219	28	11	14			
C_{42}	0.64150	1.1130	0.07902	0.00198	0.00098	0.000125	-------	-------	-------
	1066	1669	844	31	13	12			

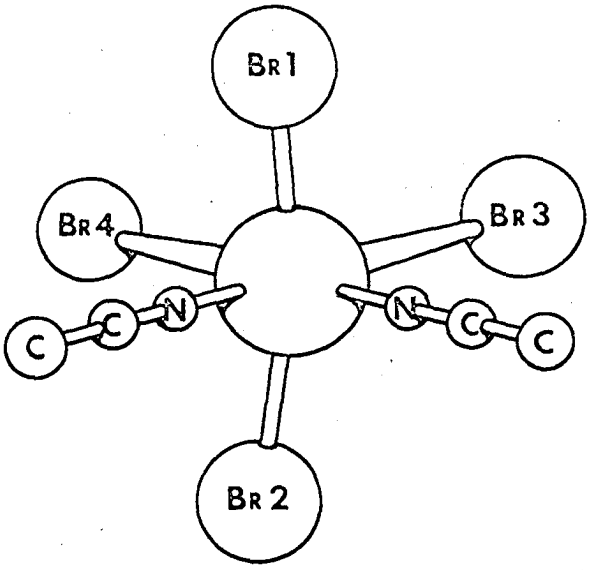

Bond Distances (Avg.)

Atoms	Dist. A°	Error A°
Nb-Br	2.48	0.01
Br-Br	3.70	0.01
Nb-N	2.03	0.10
N-C_{cn}	1.16	0.14
C_{cn}-C_{ch3}	1.47	0.15

Bond Angles

Atoms	Angle°	Error°
Br_t-Nb-Br_t	159.3	0.4
Br_c-Nb-Br	96.7	0.8
Br-Nb-N	83.5	3.5
N-C-C	174	8.6

Figure 8. The $NbBr_4(CH_3CN)_2$ molecule

Table 7. Intramolecular distances and errors

Atoms	Dist. (Å)	Stnd. dev.
$Nb-Br_1$	2.47	0.02
$Nb-Br_2$	2.50	0.02
$Nb-Br_3$	2.47	0.02
$Nb-Br_4$	2.49	0.02
Nb-N	2.03*	0.10
N-C	1.09*	0.14
C_1-C_2	1.47*	0.15
Br_1-Br_2	4.88	0.02
Br_2-Br_3	3.71	0.02
Br_2-Br_4	3.74	0.02
Br_1-Br_3	3.69	0.02
Br_1-Br_4	3.71	0.02
Br_3-Br_4	3.68	0.015

*Average of three

Table 8. Interatomic angles and errors

Defining atoms	Angle°	Stnd. dev.
$Br_1-Nb-Br_2$	159.3	0.4
$Br_2-Nb-Br_3$	97.5	0.7
$Br_2-Nb-Br_4$	98.0	0.8
$Br_1-Nb-Br_3$	96.0	0.8
$Br_1-Nb-Br_4$	96.1	0.7
$Br_3-Nb-Br_4$	96.1	0.5
Br_1-Nb-N_3	83.6	3.4
Br_1-Nb-N_4	81.9	3.3
Br_1-Nb-N_3	82.6	3.5
Br_1-Nb-N_4	84.0	3.2
Br_3-Nb-N_3	178.1	3.7
Br_3-Nb-N_4	83.8	3.7
Br_4-Nb-N_3	85.3	3.6
Br_4-Nb-N_4	179.8	3.4
$Nb-N_3-C_{31}$	172	7.6
$Nb-N_4-C_{41}$	175	11.1

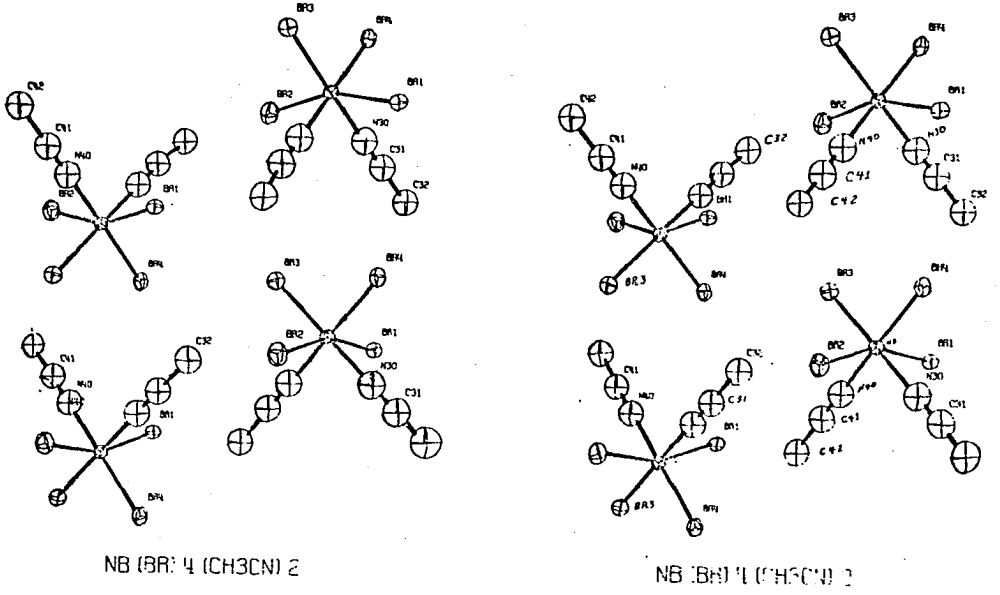

Figure 9. A three-dimensional representation of the $NbBr_4(CH_3CN)_2$ structure

is 2.48 ± 0.01Å. The cis and trans bond lengths are identical within experimental error. The only other known measurement of this distance is that of Skinner and Sutton (55). Their electron diffraction studies of $NbBr_5$ gas yielded values of 2.46 ± 0.05Å. One might expect slightly reduced radii for the $NbBr_5$ molecule due to the increased charge on the central atom. The intramolecular Br-Br distance of 3.50Å in $NbBr_5$ is much shorter than the 3.68Å minimum Br-Br distance of this determination. The former figure was estimated using 90° Br-Nb-Br angles. These angles are considerably distorted from 90° in this determination however. It is tempting to speculate that the higher coordination number and lower symmetry of $NbBr_4(CH_3CN)_2$ is responsible for the disparity of Nb-Br bond distances and angles. In view of the relatively large error in the $NbBr_5$ determination however, the possibility that these distances are identical in both determinations cannot be ruled out. Using 1.14Å for the "tetrahedral covalent radius of the bromine atom" (56) and the 2.48Å average Nb-Br distance of this determination, we find the radius of niobium(IV) to be 1.34Å in these complexes.

The carbon and nitrogen atom placement is poor in this

determination. This is in part due to the nature of the experiment and in part due to inadequate handling of the low intensity data. The electron density function was defined in an earlier section as

$$\rho(x,y,z) = \frac{1}{V} \sum_{h} \sum_{k} \sum_{\ell} F(hk\ell) \exp\left[-2\pi i (hx+ky+\ell z)\right] .$$

Inverting this series and substituting for known quantities,

$$F(hk\ell) = \sum_{n} Z_n \exp\left[2\pi i (hx_n+ky_n+\ell Z_n)\right] ,$$

where the summation is over the n atoms of the unit cell and Z_n is the atomic number of the nth atom. For a general value of $\{hk\ell\}$, the magnitude of $F(hk\ell)$ is principally determined by the niobium and bromine atom positions. The weak reflections are determined by light atom positions, but the intensities of these reflections are least accurately known. Thus, light atoms are difficult to place accurately in any structure containing many heavy atoms. Better agreement for weak intensities is gotten by measuring the area under the intensity curve recorded on chart paper, and scaling these data in with the moderate and high intensity reflections.

In the light of the above considerations, little quantitative information can be learned about the acetonitrile

molecules. Other determinations give quite similar results. Willet and Rundle (57) reported the structures of $Cu_2Cl_4(CH_3CN)_2$ and $Cu_3Cl_6(CH_3CN)_2$ which contain similarly coordinated acetonitrile groups. Their values of 1.16Å for the N-C and 1.47Å for C-C bond distances and 178° for the C-C-N angle compare with the corresponding values 1.09Å, 1.47Å and 172° for this structure. Willet and Rundle conclude that the non-linear Cu-N-C angle indicates partial use of the Sp2 hybrid orbitals by the nitrogen atom. Cotton and Lippard find corresponding values of 1.22Å, 1.46Å and 179° in a recent investigation of the tetraphenylarsonium oxotetrabromoaceto-nitrilerhenate(V) structure (58). They report the Re-N-C angle of 170°. Due to the uncertainty in locating light atom positions (vide supra) these results may not be significant.

The niobium atom, the cis bromine pair and the nitrogen atoms are coplanar. Table 9 gives the equation of the least square plane through these atoms with the distance of all atoms from this plane. The plane determined by the niobium atom and the trans bromine pair is also given. The dihedral angle between these planes is 86.0 ± 3 degrees.

The niobium-nitrogen distance is 2.02 ± 0.10Å. This gives 0.68Å for the coordination radius of nitrogen in this

Table 9. Least square plane equation and atom deviations (Angstroms)
A $0.0190x + 0.7289y + 0.6844z - 6.264 = 0$
B $0.0493x - 0.6821y + 0.7296z + 0.36717 = 0$

	ΔA	ΔB
Nb	-0.00*	-0.00*
Br_1	2.42	0.00
Br_2	-2.46	0.00
Br_3	0.00*	-1.84
Br_4	0.00*	-1.86
N_3	0.00*	1.50
N_4	0.00*	-1.51
C_{31}	-0.00	-2.35
C_{32}	0.00	-3.51
C_{41}	0.00	2.32
C_{42}	-0.00	3.47

*Asterisked atoms define plane.

structure. A similar value for the $Cu_2Cl_4(CH_3CN)_2$ structure is 0.68Å, while Cotton *et al.* (58) find 0.93Å. These latter authors ascribe this large elongation to the weakening of the Re-N bond by triple bond character of the opposing oxygen atom. Even with the large probable error present in these determinations, one must presume that the Re-N bonding is far weaker than the Nb-N interaction within this structure.

Study of the three-dimensional representation of the unit cell and of Table 7 (b) indicates that the molecular structure is not distorted by packing within the crystal. The closest intermolecular distance is 3.78 ± 0.13Å for the

methyl carbon of one molecule and a bromine of another. The van der Waals radius of bromine is 1.95Å and that of a methyl group is 2.00Å.

PART II. INFRARED SPECTRA

INTRODUCTION

Since accurate information about the structure of $NbBr_4(CH_3CN)_2$ had become available, it was of interest to study the infrared spectra of the $NbX_4(CH_3CN)_2$ compounds and attempt to make a more complete assignment of the bands therein.

A normal coordinate analysis of the octahedral species L_2MX_4 has been calculated by Beattie et al. (59). This analysis indicates significant differences in the vibrational spectra of the cis and trans isomers. The reducible representation for the metal-halogen stretching modes of the cis (C_{2v}) molecule is

$$\Gamma_{cis}\ (\text{M-X str}) = 2A_1 + B_1 + B_2.$$

These modes are all infrared active so four M-X stretching frequencies might be observed in the infrared spectrum. Beattie's calculations indicate that three M-X stretching modes might occur together at higher frequencies, with the fourth band at considerably lower energies in the far infrared region of the spectra. The metal-ligand representation is

$$\Gamma_{cis}\ (\text{M-L str}) = A_1 + B_2.$$

Thus two M-L stretching bands might be observed, since both modes are infrared active.

The trans (D_{4h}) molecule has the representations

$$\Gamma'_{trans}\ (M\text{-}X\ str) = E_u + A_{1g} + B_{1g},\ and,$$

$$\Gamma'_{trans}\ (M\text{-}L\ str) = A_{1g} + A_2\ .$$

The A_{1g} and B_{1g} modes are infrared inactive so only one metal-halogen and one metal-ligand mode should appear in the spectrum of the trans isomer.

The representations for the LMX_5 molecule (C_{4v}) are

$$\Gamma''(M\text{-}X\ str) = 2A_1 + B_1 + E,\ and$$

$$\Gamma''(M\text{-}L\ str) = A_1.$$

Only the B_1 representation is infrared inactive; therefore one metal-ligand stretching mode and three metal-halogen stretching modes are contained in the spectrum.

It has not been established where the M-N stretching frequency occurs for such nitrile complexes, nor for the N-C-CH_3 bending modes. Moreover, the spectra of cis-coordinated, bis-nitrile adducts of this type characteristically exhibit only one C-N stretching band whereas two should appear (60). A thorough understanding of these spectra could enable future workers to reliably determine molecular configuration for such complexes by study of the vibrational spectra.

EXPERIMENTAL

Solid complexes were prepared in the manner of Torp (10) by extraction of the metal halide with its corresponding ligand. The CD_3CN, obtained from Merck, Sharp and Dohme of Canada Limited, was outgassed to 10^{-5} Torr., dried over P_2O_5, and stored over $NbCl_5$. Outgassed nujol was refluxed over sodium metal and stored in an argon drybox until used. Hexachlorobutadiene was outgassed and dried over molecular sieves and a $NbBr_4(CH_3CN)_2$ mull was prepared for examination of the CH_3 deformation region of its spectrum. All other samples were prepared in nujol mulls for examination of their spectra. This was done in an argon drybox and the mulls were sealed in a special cell-holder so that moisture and air were excluded. Polyethylene windows were used for recording the far infrared spectra of these materials with a Beckman IR-11 instrument. Potassium bromide windows were used for the near-infrared region which was recorded by a Beckman IR-7 instrument. The frequencies quoted are accurate to $\pm$ 2 $cm.^{-1}$.

RESULTS AND DISCUSSION

The infrared data for these complexes are divided into two regions, 650-2500 $cm.^{-1}$, and 50-650 $cm.^{-1}$, which will be discussed separately. The spectra of these complexes in the range 800-2500 $cm.^{-1}$ all arise from coordinated acetonitrile and hence are all very similar. This is true of the deuterated complexes as well.

The spectra of $NbBr_4(CH_3CN)_2$ and of $NbBr_4(CD_3CN)_2$ are shown in Figure 10. The following discussion relates primarily to these complexes though others will be discussed. The "breaks" in the curves of Figures 10 and 11 indicate a change in filters, mulls, or in the abscissa. The bands, their intensities and assignments are listed in Table 10 for all complexes studied in this investigation.

The vibrational spectra of CH_3CN and of CD_3CN are well understood and the assignments are essentially complete (61, 62). The fundamental vibration frequencies, assignments and types of motion for these ligands are given in Table 11.

The near-infrared spectra of the complexed nitriles show that they do not depart significantly from the free C_{3v} molecule. No splitting of the doubly degenerate modes is observed. In the C-N stretching region for $NbBr_4(CH_3CN)_2$ there

Figure 10a. The near infrared spectrum of $NbBr_4(CD_3CN)_2$

Figure 10b. The near infrared spectrum of $NbBr_4(CH_3CN)_2$

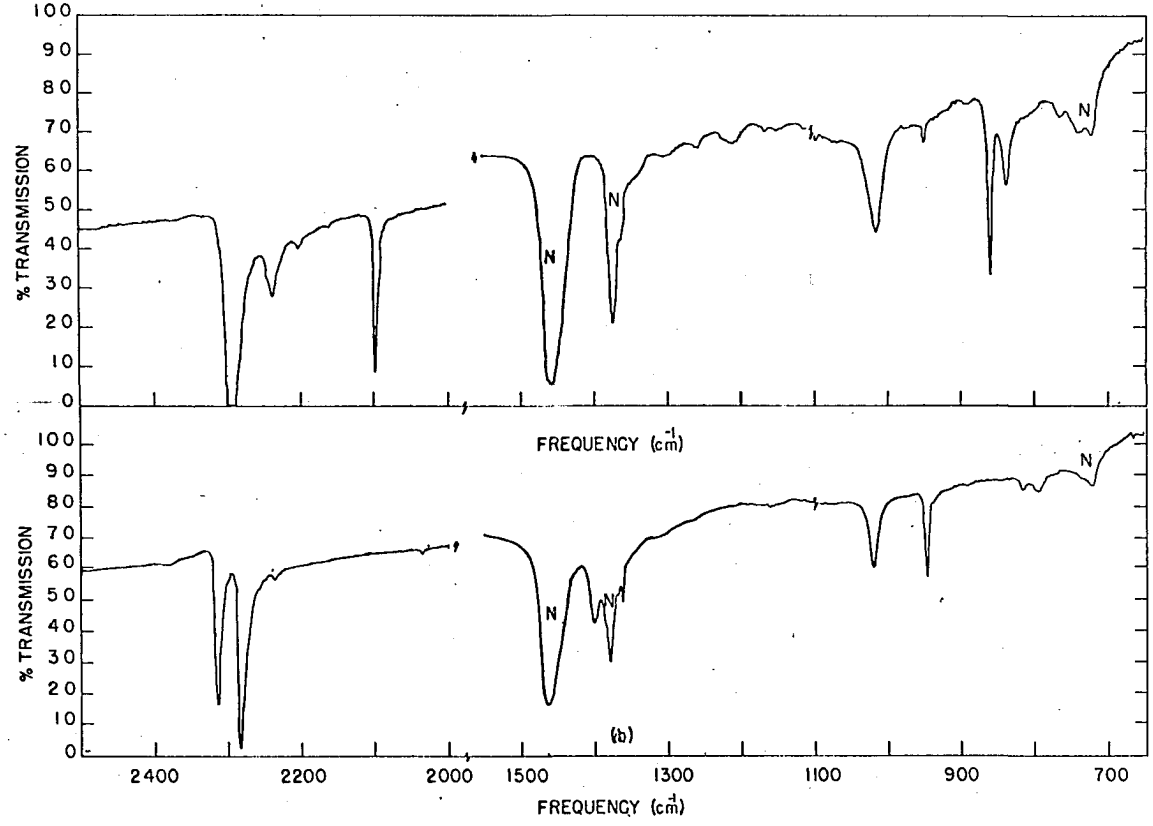
% TRANSMISSION
100
90
80
70
60
50
40
30
20
10
0
N
N
N
FREQUENCY (cm⁻¹)
% TRANSMISSION
N
N
N
(b)
2400
2200
2000
1500
1300
1100
900
700
FREQUENCY (cm⁻¹)

Table 10. Vibration frequencies (750-2500 cm^{-1})

Assignment	$NbBr_4(CH_3CN)_2$	$NbBr_4(CD_3CN)_2$	$NbBr_5(CH_3CN)$	$NbBr_5(CD_3CN)$	$NbCl_4(CH_3CN)_2$	$NbCl_5(CH_3CN)$
$2\nu_8$	798vw 819vw	738vw 763vw	801w 812vw	733vw 755sh.vw	804m 825vw	808w 817sh,vw
ν_4	950vs	838m	946vs	840m	952s	949vs
ν_7	1023s	860s	1022s	857s	1030s	1026s
ν_6	1400m	1016s	1399w	1013s	1406w	1402m
ν_3	1359w	---	1359m,sharp	---	1367w,sharp	1361m
$\nu_7+\nu_8$	1442[a]	---	---	---	---	---
ν_1	---	2098s	---	2096s	---	---
ν_2' [b]	2239vw	---	2248vvw	---	2243vw	2253vw
ν_5	---	2239m	---	2238m	---	---
ν_2	2286vs	2295vs	2287vs	2308vs	2290vs	2294vs
	---	---	---	---	2314sh	---
$\nu_3+\nu_4$	2317vs	---	2315vs	---	2320vs	2322vs

[a]Observed only in halocarbon mull.

[b]Frequency of C^{13}-N stretching vibration.

Table 11. Fundamental frequencies of CH_3CN and CD_3CN vapor

Assignment	Type of motion	CH_3CN (cm^{-1})[a]	CD_3CN (cm^{-1})[b]
$\nu_1(A_1)$	C-H stretch	2954	2126
$\nu_2(A_1)$	C≡N stretch	2267	2278
$\nu_3(A_1)$	CH_3 deformation	1389	~1110
$\nu_4(A_1)$	C-C stretch	920	831
$\nu_5(E)$	C-H stretch	3009	2257
$\nu_6(E)$	CH_3 deformation	1454	1046
$\nu_7(E)$	CH_3 rock	1041	847
$\nu_8(E)$	C-C≡N bend	361	331

[a]Venkateswarlu and Thanalkshmir (61).

[b]Fletcher *et al.* (62).

exist two strong bands at 2317 and 2286 $cm.^{-1}$. The band at 2317 $cm.^{-1}$ appears to arise from a combination mode involving the CH_3 deformation at 1362 $cm.^{-1}$ and the symmetric C-C stretch at 950 $cm.^{-1}$. Other authors have considered this mode and ascribe its intensity to either Fermi resonance with the lower frequency C-N stretch or to an effect of mechanical coupling (63,64). These three modes are all of identical symmetry (A_1) as they must be to form combination modes or to exhibit Fermi resonance. Examination of this region in the deuterated complex supports these suppositions since the band arising from the combination mode is absent.

The C-N stretching frequencies are shifted 20-30 $cm.^{-1}$ to higher frequencies in these complexes. This phenomena is well known in other nitrile complexes (65,66). Beattie et al. (59) ascribed these shifts to M-N coordination through the non-bonding electron pair of nitrogen which results in strengthening of the C-N bond.

The region 1350-1500 $cm.^{-1}$ is badly obscured by nujol absorption bands. A halocarbon mull of $NbBr_4(CH_3CN)_2$ was prepared and absorption bands were observed at 1359, 1400 and 1442 $cm.^{-1}$. Clearly the CH_3 deformation is shifted by 30 $cm.^{-1}$ to lower energies upon coordination in $NbBr_4(CD_3CN)_2$.

Similar behavior is expected in the acetonitrile complex so the 1359 $cm.^{-1}$ peak is assigned as the symmetric CH_3 deformation. The antisymmetric CH_3 deformation acts similarly and may occur at 1400 $cm.^{-1}$. The peak at 1442 $cm.^{-1}$ appears to be a $\nu_7+\nu_8$ combination band strengthened by Fermi resonance. The assignment of the ν_6 and the $\nu_7+\nu_8$ bands is tenuous. It is difficult to establish unambiguously which peak is which due to the resonance interaction between them. Actually, the peaks are each mixtures of the ν_6 and the $\nu_7+\nu_8$ modes.

Three very weak, broad bands appear at ca. 1214, 1262, and 1304 $cm.^{-1}$ respectively in the $NbBr_4(CD_3CN)_2$ spectra. This is the strongest spectrum observed so these bands may stem from the complex or from impurities. Combination modes of $\nu_7+\nu_8$ may appear in this region; if so, from use of the fundamental frequencies they should appear at 1227, 1237 and 1244 $cm.^{-1}$. These bands do not appear in the $NbBr_5(CD_3CN)$ spectrum.

Two sharp bands occurring at 1023 and 950 $cm.^{-1}$ respectively in the $NbBr_4(CH_3CN)_2$ spectrum are assigned as the CH_3 rocking mode and the C-C stretching mode. These peaks are shifted to higher energies by coordination. The analogous

CD_3 rocking mode at 860 $cm.^{-1}$, and the C-C stretching mode, at 838 $cm.^{-1}$, are shifted sharply to lower frequencies by the isotope effect in the deuterated complex. A sharp, weak peak appears at 950 $cm.^{-1}$ in the deuterated complex. It is not clear whether this indicates impurities in the sample or is part of the spectrum. This peak does not appear in the $NbBr_5(CD_3CN)$ spectrum.

Two very weak, very broad bands appear in the $NbBr_4(CH_3CN)_2$ spectrum at ca. 798 and 819 $cm.^{-1}$ respectively. These appear to be overtones of the CH_3-C-N bending modes to be discussed in the next section. Analogous peaks occur for the deuterated specie at ca. 738 and 763 $cm.^{-1}$. These latter peaks are slightly obscured by the nujol band at 723 $cm.^{-1}$.

The far infrared spectra (150-650 $cm.^{-1}$) are depicted for $NbBr_4(CH_3CN)_2$ and $NbBr_4(CD_3CN)_2$ in Figure 11. A listing of the spectra (50-650 $cm.^{-1}$) for all complexes studied in this investigation is given in Table 12.

In the spectrum of CH_3CN the fundamental CH_3-C-N bending mode was calculated from the observed frequency of the overtone $2\nu_8$, to occur at 361 $cm.^{-1}$ (67). Since the C-N stretching frequency of a coordinated nitrile is observed at higher energy, and the C-N bond appears stronger in the

Figure 11a. The far infrared spectrum of $NbBr_4(CH_3CN)_2$

Figure 11b. The far infrared spectrum of $NbBr_4(CD_3CN)_2$

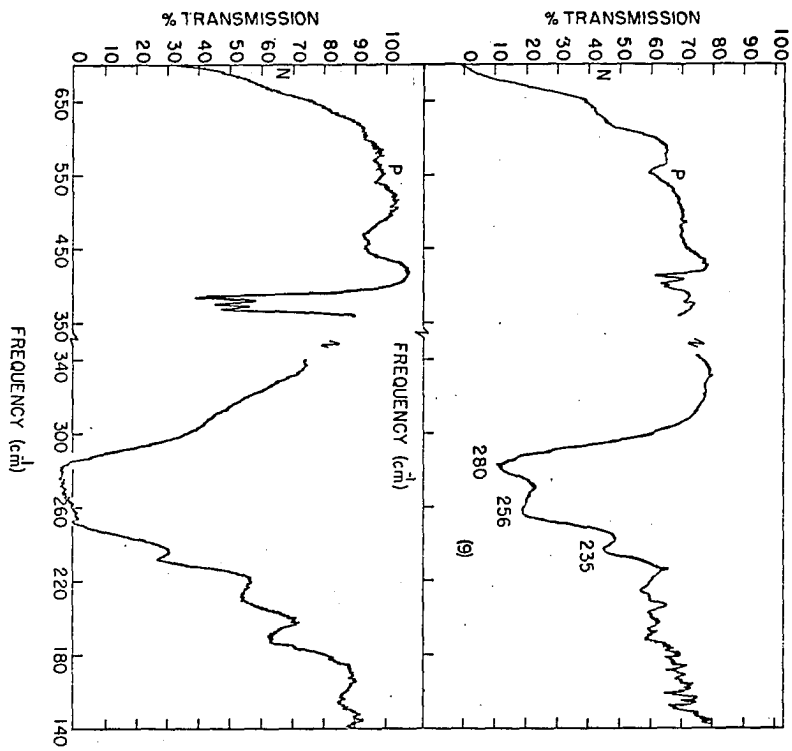
% TRANSMISSION
100
90
80
70
60
50
40
30
20
10
0
N
P
280
256
235
(9)
FREQUENCY (cm⁻¹)
650
550
450
350
340
300
260
220
180
140

Table 12. Vibrational spectra (40-650 $cm.^{-1}$)

$NbBr_4(CH_3CN)_2$	$NbBr_4(CD_3CN)_2$	$NbCl_4(CH_3CN)_2$	$NbBr_5(CH_3CN)$	$NbBr_5(CD_3CN)$	$NbCl_5(CH_3CN)$
99 w,brd	82 m,brd 94m,brd	91 m	83 vw	94 w,v brd	
114 vw,brd	154 w,brd	115 w,brd	109 vs,v brd	107 m,v brd	112 s, brd
	184 w,sh	139 vs	172 w,brd	185 m,v brd	160 vs
	189 m	197 m,brd	195 s	196 m,v brd	195 m,sh
213 w,shrp	212 m,brd	213 m	210 s	228 w,v brd	215 s,brd
	218 s,brd				244 m
235 s	232 s	248 m			297 m
256 vs	252-286	334 vvs,brd	240-310	245-300	350-440 [a]
280 vs	vvs and	365 vvs,brd	vvs and	vvs and	vvs and
	vv brd		vv brd	vv brd	vv brd
376 vw					
396 m	367 s,shrp	400 m,sh	401 s, shrp	375 s,shrp [b]	
401 m	377 s,shrp	411 m,sh	406 s,shrp	381 s,shrp	
411 m	384 s,shrp				
	450 w,brd		466 vw	455 m,brd	
	466 w,brd				

vs - very strong
s = strong
m = medium
w = weak

vw = very weak
brd - broad
shrp = sharp
sh = shoulder

[a] Nb-X stretching modes.

[b] CH_3-C-N bending modes.

coordinated nitrile, it should be expected that the CH_3-C-N bending modes would also occur at higher energies. Four weak bands occur at 376, 396, 401 and 411 $cm.^{-1}$ in the $NbBr_4(CH_3CN)_2$ spectrum. $NbCl_4(CH_3CN)_2$ has two weak bands at 400 and 411 $cm.^{-1}$ but since they appear only as shoulders on the more intense band arising from the M-Cl stretching vibration, the same degree of resolution as in the bromine complex was not attained. This region of the $NbCl_5(CH_3CN)$ spectrum is completely dominated by the M-Cl stretching band, but the $NbBr_5(CH_3CN)$ spectrum shows two intense bands at 401 and 406 $cm.^{-1}$. Direct comparison of these spectra with the spectra of the deuterated analogs strongly indicates that these bands do arise from the CH_3-C-N bending modes. The three highest bands of the tetrabromide complex and the two bands of the pentahalide complexes are shifted to lower frequency by 25-30 $cm.^{-1}$ in each case.

The $NbBr_4(CH_3CN)_2$ spectrum contains three intense bands at ca. 235, 256 and 280 $cm.^{-1}$. These bands appear to remain unshifted upon deuteration of the complex. The $NbBr_5(CH_3CN)$ spectrum shows a very intense absorption band extending from ca. 250-300 $cm.^{-1}$ which also appears unaffected by deuteration. In view of the great strength of these bands, their insensi-

tivity to deuteration, and to their presence in both tetra- and penta-halide complexes, the bands are assigned as Nb-Br stretching frequencies.

The chloro-analogs of these acetonitrile complexes have very intense bands extending from ca. 320-380 $cm.^{-1}$ in $NbCl_4(CH_3CN)_2$, and from ca. 330-400 $cm.^{-1}$ in the $NbCl_5(CH_3CN)$ complex. Thus the Nb-Cl stretching frequencies are assigned to the region 320-400 $cm.^{-1}$. The extreme intensity and width of these bands eliminates the possibility of determining the number or exact location of these stretching modes.

Many other bands have been observed in the region below 300 $cm.^{-1}$. Reliable assignments of these bands would require extension of the normal coordinate analysis of Beattie as well as lengthy and detailed calculations. It is in this region that the metal-nitrogen stretching and metal-halogen or metal-nitrogen bending frequencies should be observed. It has been definitely established from this study that the metal-nitrogen stretching frequency must occur below ca. 400 $cm.^{-1}$ since all bands at higher frequencies have been assigned with confidence.

The occurrence of three CH_3-C-N bending frequencies in the $NbBr_4(CH_3CN)_2$ complex and of two in the NbX_5CH_3CN com-

plex and of two in the NbX_5CH_3CN complexes is of interest. The C_{2V} symmetry group contains only two infrared active bending modes and the C_{4V} group contains one. These modes are expected to have extreme dependence upon their environment; thus, multiplicity of modes may be indicative of pseudo-C_{2V} symmetry in the $NbBr_4(CH_3CN)_2$ molecule. Slight deviations of the acetonitrile molecules from positions giving true C_{2V} symmetry may split the vibrational energy levels to give this effect. The occurrence of two bending modes in the NbX_5CH_3CN spectra may be due to a similar effect, or to conditions of "site symmetry" within the solid (12).

SUMMARY

The structure of tetrabromobis(acetonitrile)niobium(IV) has been determined by x-ray diffraction techniques. Single crystals were grown from acetonitrile solution. The compound crystallizes in the orthorhombic space group $Pna2_1$, with lattice parameters a = 13.92 ± 0.01, b = 6.58 ± 0.01 and c = 13.63 ± 0.01 angstroms.

This complex is a slightly distorted octahedron with the acetonitrile groups bonded to niobium through the nitrogen atoms in cis positions. The trans and cis Nb-Br bond lengths were found to be identical within experimental error; the average value was 2.48 ± 0.01 angstroms. Interatomic repulsions between bromine atoms appear to distort all Br-Nb-Br from the expected 90° to ca. 97° for the cis bromine atoms. The Nb-N bond length is 2.0 angstroms. No abnormalities are noted for the ligand bond lengths or angles.

The infrared spectra (50-2500 $cm.^{-1}$) have been measured for $NbX_4(CH_3CN)_2$, $NbX_5(CH_3CN)$ (X = Cl, Br) and the deuterated bromide analogs. The niobium-bromine stretching modes have been assigned to the region 250-310 $cm.^{-1}$ while the niobium chlorine stretching region is 330-420 $cm.^{-1}$. The $NbBr_4(CH_3CN)_2$ complex has three CH_3-C-N bending modes at ca. 400 $cm.^{-1}$. The

$NbBr_5(CH_3CN)$ complex has two CH_3-C-N bending modes at this position. These bending modes were shifted to lower frequencies by *ca.* 25 $cm.^{-1}$ upon substitution of CD_3CN for CH_3CN in the complexes.

BIBLIOGRAPHY

1. McCarley, R. E. and Torp, B. A. Inorg. Chem. 2, 540 (1963).

2. McCarley, R. E. and Boatman, J. C. Inorg. Chem. 2, 547 (1963).

3. Horner, S. M. and Tyree, S. Y. Inorg. Chem. 2, 568 (1963).

4. Allen, E. A., Edwards, D. A. and Fowles, G. W. A. Chem. Ind. 1962, 1026 (1962).

5. Lewis, I., Machini, D. J., Newnham, I. E. and Nyholm, R. S. J. Chem. Soc. 1962, 2036 (1962).

6. Wentworth, R. A. D. and Brubaker, C. H. Inorg. Chem. 2, 551 (1963).

7. Wentworth, R. A. D. and Brubaker, C. H. Inorg. Chem. 3, 47 (1964).

8. Fowles, G. W. A. and Hoodless, R. A. J. Chem. Soc. 1963, 33 (1963).

9. Clark, R. J. H., Lewis, J., Machin, D. J. and Nyholm, R. S. J. Chem. Soc. 1963, 379 (1963).

10. Torp, B. A. Spectra, magnetic susceptibilities and structure of some halogen complexes of niobium(IV) and tantalum(IV). Unpublished Ph.D. thesis. Ames, Iowa, Library, Iowa State University of Science and Technology. 1964.

11. Ballhausen, C. J. Introduction to ligand field theory. New York, New York, McGraw-Hill Book Co., Inc. 1962.

12. Cotton, F. A. Chemical applications of group theory. New York, New York, Interscience Publishers, Inc. 1963.

13. H. D. Bedon, W. E. Hatfield, S. M. Horner, and S. Y. Tyree, Jr., Inorg. Chem. 5, 743 (1965).

14. H. D. Bedon, S. M. Horner, and S. Y. Tyree, Jr. Inorg. Chem. 3, 647 (1964).

15. Ballhausen, C. I. and Gray, H. B. Inorg. Chem. 1, 111 (1962).

16. Wells, A. F. Structural inorganic chemistry. 3rd ed. London, England, Oxford University Press. 1962.

17. Dunn, T. M. Trans. Faraday Soc. 57, 1441 (1961).

18. H. Schäfer and K. D. Dokmann. Z. anorg. allgem. Chem. 299, 197 (1959).

19. H. Schäfer and L. Bayer. Z. anorg. allgem. Chem. 277, 140 (1954).

20. J. D. Corbett and P. Seabaugh. J. Inorg. Nucl. Chem. 6, 207 (1958).

21. P. Seabaugh. Physical properties of niobium iodides. Unpublished Ph.D. thesis. Ames, Iowa, Library, Iowa State University of Science and Technology. 1961.

22. L. Dahl and D. Wampler. J. Am. Chem. Soc. 81, 3150 (1959).

23. V. Gozzi and S. Vivarelli. Z. anorg. allgem. Chem. 279, 165 (1955).

24. Korshunov, B. G. and Safonov, V. V. Russian Journal of Inorganic Chemistry 6, 385 (1961).

25. Korschunov, B. G., Safonov, V. V. and Sheutsoug, Z. N. Russian Journal of Inorganic Chemistry 7, 1021 (1962).

26. P. G. Rasmussen, H. A. Kuska, and C. H. Brubaker, Jr. Inorg. Chem., 4, 343 (1965).

27. Allbutt, M., Feenan, F., and Fowles, G. W. A. J. Less-Common Metals 6, 299-306 (1964).

28. Clark, R. J. H., Kepert, D. L., Lewis, J., and Nyholm, R. S., Jr. J. Chem. Soc. 1965, 2865 (1965).

29. Williams, D. E. and Rundle, R. E. J. Am. Chem. Soc. 86, 1660 (1964).

30. Granoff, B. The crystal and molecular structures of dicarbonyl-π- cyclopentadienylbicyclo(2·2·1) hepta-2π, 5-dienemanganese(I) and tetrabutyl ammonium tris acetylacetonatocobalt(2). Unpublishes Ph.D. thesis. Princeton, New Jersey, Library, Princeton University. 1966.

31. Johnston, T. E. Patterson I. Ames Lab. Computer Library, Ames, Iowa. 1964.

32. Erbeck, D. Veccheck. Ames Lab. Computer Library, Ames, Iowa. 1965.

33. Busing, W. R. and Levy, H. A. Acta Cryst. 10, 180 (1957).

34. Busing, W. R., Martin, K. O., and Levy, H. A. U.S. Atomic Energy Commission Report ORNL-TM-305 [Oak Ridge National Laboratory, Tenn.] 1962.

35. Busing, W. R., Martin, K. O., and Levy, H. A. U.S. Atomic Energy Commission Report ORNL-TM-306 [Oak Ridge National Laboratory, Tenn.] 1964.

36. Johnson, C. K. U.S. Atomic Energy Commission Report ORNL-3794 [Oak Ridge National Laboratory, Tenn.] 1966.

37. Lipson, H. and Cochran, W. The determination of crystal structures. London, England, G. Bell and Sons, Ltd. 1953.

38. Woolfson, M. M. Direct methods in crystallography. London, England, Oxford University Press. 1961.

39. Wrinch, D. M. Phil. Mag. 27, 98 (1939).

40. Buerger, M. J. Acta Cryst. 3, 87 (1950).

41. McLachlan, D. Proc. Nat. Acad. Sci. 37, 115 (1951).

42. Fridrichsons, J. and McL. Mathieson, A. Acta Cryst. 15, 1065 (1962).

43. Simpson, P. G., Dobrott, R. D., and Lipscomb, W. N. Acta Cryst. 18, 169 (1965).

44. Patterson, A. L. Phys. Rev. 46, 372 (1934).

45. Buerger, M. J. Vector space and its application in crystal-structure investigation. New York, New York, John Wiley and Sons Co. 1959.

46. Buerger, M. J. Proc. Nat. Acad. Sci. 36, 376 (1950).

47. International tables for x-ray crystallography. Vol. 1. Birmingham, England, Kynoch Press. 1952.

48. Mighell, A. D. and Jacobson, R. A. Acta Cryst. 17, 1554 (1964).

49. McLachlam, D. Crystal structure determinations. New York, N.Y., McGraw-Hill Book Company, Inc. 1957.

50. Furnas, T. C., Jr. Single crystal orienter instruction manual. Milwaukee, Wisconsin, General Electric Company. 1957.

51. International tables for x-ray crystallography. Vol. 3. Birmingham, England, Kynoch Press. 1962.

52. Beers, Y. Introduction to the theory of error. Reading, Massachusetts, Addison-Wesley Publishing Co., Inc. 1962.

53. Hansen, H. P., Herman, F., Lea, J. D., and Skillman, S. Acta Cryst. 17, 1040 (1964).

54. Cruickshank, D. W. J. and Pilling, D. E. Computing methods and the phase problem in x-ray crystal analysis. New York, New York, Pergamon Press, Inc. 1961.

55. Skinner, H. A. and Sutton, L. E. Trans. Faraday Soc. 36, 668 (1940).

56. Pauling, L. The nature of the chemical bond. 3rd ed. Ithaca, N.Y., Cornell University Press. 1960.

57. Willet, R. D. and Rundle, R. E. J. Chem. Phys. 40, 838 (1964).

58. Cotton, F. A. and Lippard, S. J. Inorg. Chem. 5, 416 (1966).

59. Beattie, I. R., Webster, M., and Chantry, G. E. J. Chem. Soc. 1964, 6172 (1964).

60. Walton, R. A. Quart. Rev. (London) 19, 126 (1965).

61. Venkateswarlu, K. and Thanalkshmir, R. Indian J. Pure Appl. Phys. 1, 64 (1963).

62. Fletcher, W. H., Shoup, C. S., and Thompson, W. T. Spectrochim. Acta 20, 1065 (1964).

63. Evans, J. C. and Lo, G. Y. Spectrochim. Acta 21, 1033 (1965).

64. Brown, T. L. and Kubota, M. J. Am. Chem. Soc., 83, 4175 (1961).

65. Beattie, I. R. and Gilson, T. J. Chem. Soc. 1964, 2293 (1964).

66. Purcell, K. F. and Drago, R. S. J. Am. Chem. Soc. 88, 919 (1966).

67. Evans, J. C. and Bernstein, H. J. Can. J. Chem. 33, 1746 (1955).

ACKNOWLEDGEMENTS

The author wishes to express his deep appreciation to Dr. R. E. McCarley for his interest, suggestions and guidance during the course of this work.

Many thanks also go to the members of P. and I. Group X for the exchange of equipment and criticism (sometimes constructive) without which this work would not have been possible. Special thanks to Miss Verna Thompson for typing duties far beyond the call of duty.

Finally, the patience and encouragement of my wife was most helpful during the course of this research.